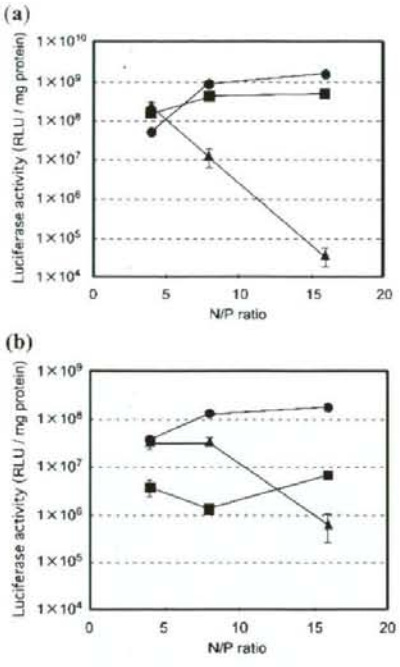

Figure 4. In vitro transfection of Huh-7 (a) and HUVEC (b) with PAsp(DET), PAsp(DPT), and BPEI polyplexes at varying N/P ratios evaluated by luciferase assays: (●) PAsp(DET), (▲) PAsp(DPT), and (■) BPEI. Results were expressed as mean ± SEM ($n = 4$).

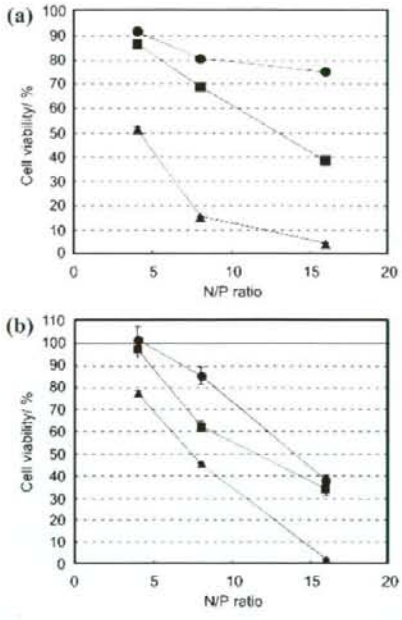

Figure 5. MTT cytotoxicity of Huh-7 (a) and HUVEC (b) with PAsp(DET), PAsp(DPT), and BPEI polyplexes evaluated under the same experimental conditions as in Figure 4 (luciferase assay): (●) PAsp(DET), (▲) PAsp(DPT), and (■) BPEI. Results were expressed as mean ± SEM ($n = 4$).

There are several key steps in the transfection process of an exogenous gene, such as cellular uptake, intracellular trafficking, release of the gene from the complexes, transcription, and translation. Furthermore, excess polycationic charge with polyplexes is an issue to induce impaired cellular homeostasis, resulting in the negative influences on whole transfection steps, especially transcription and translation. Indeed, our previous study revealed that the challenge of linear PEI polyplexes into Huh-7 cells stably expressing firefly luciferase highly impaired the transcription and translation processes to reduce the expression of firefly luciferase as well as a variety of house-keeping genes.[23] In this regard, a toxicological assay was completed to explore the different transfection profiles between PAsp(DET) and PAsp(DPT) polyplexes against N/P ratio. As shown in Figure 5a,b, the results of the MTT cell viability assay, the cytotoxicity of each polyplex under the same experimental condition as the luciferase assay increased with N/P ratio for both cells, Huh-7 and HUVEC. This result is in good agreement with the result from the MTT assay of each polymer without pDNA (Supporting Figure 3a,b and Supporting Table 1, Supporting Information). Obviously, the PAsp(DET) polyplex had much lower toxicity than the PAsp(DPT) polyplex. In detail, at a N/P ratio of 16 in Huh-7 cells, the viability of cells incubated with PAsp(DET) polyplexes was over 70% of that of control cells, whereas the viability was less than 10% in the case of PAsp(DPT) polyplexes (Figure 5a). Similarly, the cytotoxicity of PAsp(DPT) polyplexes was the highest against HUVEC, followed by BPEI and PAsp(DET) polyplexes (Figure 5b). From these results, it is worth noting that only one additional methylene group between two amino groups in the side chain crucially elevates the cytotoxicity of the cationic poly(aspartamides). This high cytotoxicity of PAsp(DPT) might contribute to the dramatically decreased transfection efficacy of PAsp(DPT) polyplexes at high N/P ratios. In contrast, cytotoxicity was substantially lowered in PAsp(DET) polyplexes, allowing high transfection efficacy with the increased N/P ratio.

To explore the endosomal escaping behavior of PAsp(DET) and PAsp(DPT) polyplexes, HUVEC trafficking studies were completed with a confocal laser scanning microscope (CLSM). In this experiment, pDNA was labeled by Cy5 (red), and nucleus and late-endosome/lysosome were stained by Hoechst 33342 (blue) and LysoTracker (green), respectively. Figure 6a,e shows the intracellular distribution of BPEI polyplexes 3 and 12 h after administration, respectively, as a positive control exerting an endosomal escaping function. Obviously, the red regions surrounding the yellow regions, where Cy5-labeled pDNA was localized in late-endosomes or lysosomes, were widely observed over time. It may be reasonable to judge that these spreading red regions represent the distribution of polyplexes exiting from the late endosomal or lysosomal stage into the cytoplasm. On the contrary, the negative control, PLys polyplexes, which lack significant buffering capacity, displayed much less red regions (Figure 6d,h), suggesting the segregation of Cy5-labeled pDNA in endo/lysosomal compartments without diffusing into cytoplasm. The confocal images of the cells transfected by PAsp(DET) polyplexes (Figure 6b,f) display spreading red regions into the cytoplasm, comparable to the previously described BPEI transfection. These data indicate facilitated transport of Cy5-labeled pDNA into the cytoplasm from the endo/lysosomal compartments. The CLSM images of PAsp(DET) polyplexes are consistent with the high buffering capacity of the native polymer. Interestingly, similar diffusing red regions were also observed for PAsp(DPT) polyplexes (Figure 6c,g), suggesting that PAsp(DPT) may facilitate endosomal escape of the polyplex, despite the previously determined poor pH-buffering capacity of PAsp(DPT). Indeed, PAsp(DPT) polyplexes showed

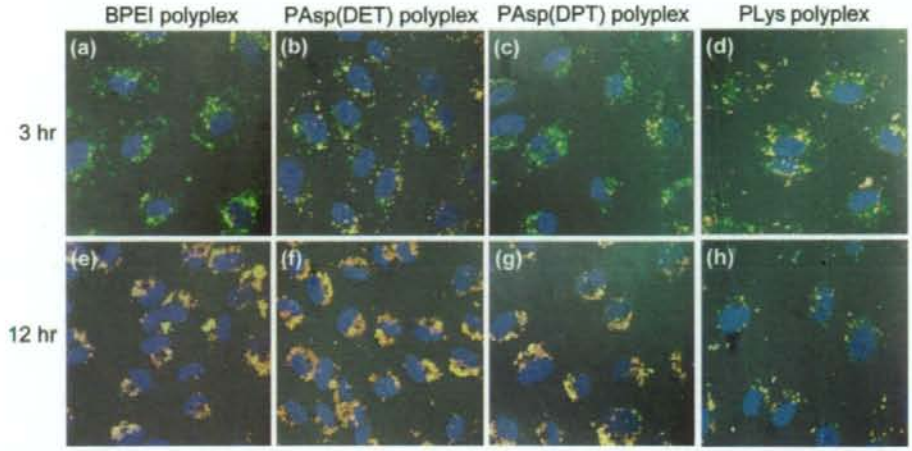

Figure 6. Intracellular distribution of Cy5-labeled pDNA complexed with a variety of polycations in HUVEC. Cy5-labeled pDNA and LysoTracker as a late-endosome and lysosome marker were observed in red and green, respectively. The cells were incubated at 37 °C for a definite time period, followed by washing with PBS, and subjected to CLSM imaging. Panels a−d and e−h are the images after 3 and 12 h incubation, respectively. (a and e) BPEI polyplexes (N/P = 8), (b and f) PAsp(DET) polyplexes (N/P = 8). (c and g) PAsp(DPT) polyplexes (N/P = 8). (d and h) PLys polyplexes (N/P = 2).

comparable transfection efficacy to BPEI and PAsp(DET) polyplexes at low N/P ratios (Figure 4a,b). These results strongly suggest the presence of another mechanism facilitating late endosomal or lysosomal escape beyond the putative proton sponge effect. Note that the medium change at 1 h after the polyplex administration significantly decreased the red regions (or dots) corresponding to endosomal escaping behavior in BPEI, PAsp(DET), and PAsp(DPT) (Supporting Figure 4, Supporting Information). This indicates that prolonged incubation of excess polyplexes with cells substantially facilitates the endosomal escape. Prolonged incubation should lead to the increased cellular uptake of polyplexes, presumably resulting in the polyplex accumulation with higher concentration in late-endosomal compartments to bring facilitated endosomal escape.

Membrane Destabilization by PAsp(DET) and PAsp(DPT). As described in the preceding section, the CLSM observation of Cy5-labeled pDNA in the intracellular compartment demonstrated that cytoplasmic transport efficiently occurred even for PAsp(DPT) polyplexes, known to possess the low buffering capacity. Of note, the previous studies addressed the destabilization of cellular membranes through the direct interaction with polycations,[5,6,28] possibly leading to the facilitated cytoplasmic transport of the polyplexes.[29−31] This destabilizing effect of polycations on the cellular membrane is considered to be dependent on the concentration (or N/P ratio), molecular weight, cationic charge density, and molecular structure of polycations.[5] Thus, the membrane destabilization induced by PAsp(DET) and PAsp(DPT) was estimated by the hemolysis assay, in which the amount of hemoglobin liberated from erythrocytes was determined from colorimetric analysis at 575 nm (Figure 7). Figure 7a clearly shows the significant difference in hemolytic activity between PAsp(DET) and PAsp(DPT) after an overnight incubation with murine erythrocytes at pH 7.4. The hemolytic activity of PAsp(DET) was negligible under the examined conditions, whereas PAsp(DPT) exhibited appreciable hemolytic activity in a concentration-dependent manner. Next, the hemolytic assays were repeated under acidic conditions indicative of the late endosomal or lysosomal state. Since overnight incubation of murine erythrocytes at pH 5.5 led to an appreciable decrease in the signal-to-noise ratio (Abs 575 nm), possibly due to instability of erythrocytes or conformational change of hemoglobins under the acidic condition, a shorter incubation time of 3 h was adopted. As clearly seen in Figure 7b, hemolytic activity levels were concentration-dependent for PAsp(DPT), regardless of the environmental pH. In direct contrast, however, the hemolytic activity of PAsp(DET) was critically enhanced by decreasing the environmental pH from 7.4 to 5.5 (Figure 7c), reaching the levels comparable to PAsp(DPT) (Figure 7b). The membrane destabilizing capacity of these polycations was further tested against HUVEC by a colorimetric LDH assay, in which the enzymatic activity of cytosolic LDH liberated from the cells was measured to estimate the membrane damages.[5,6] Figure 8a clearly shows that PAsp(DPT) induced LDH liberation in a concentration-dependent manner, both at acidic and physiological pH conditions. These data suggest a strong capacity of PAsp(DPT) to destabilize the endosomal membrane as well as the cytoplasmic membrane, regardless of the environmental pH. This is consistent with the results of the hemolysis assay shown in Figure 7b. Alternatively, the activity of LDH liberated from HUVEC incubated with PAsp(DET) was obviously low at pH 7.4, while the decrease in pH to acidic condition (pH ~5) substantially enhanced its activity to the same level as that of PAsp(DPT) (Figure 8b), exhibiting the similar trend to the hemolytic activity (Figure 7c). Similar results of the membrane destabilization were obtained for Huh-7 cells (data not shown). Apparently, the concentration-dependent increase in the membrane destabilization capacity of PAsp(DET) under the acidic condition corresponds to the enhanced transfection efficacy with N/P ratios (Figure 4).

We next sought to find a correlation between the interaction of the polycations with the membrane and the destabilization effect. CLSM observations were further carried out for HUVEC

(28) Zhang, Z.-Y.; Smith, B. D. *Bioconjugate Chem.* **2000**, *11*, 805–814.
(29) Merdan, T.; Kunath, K.; Fischer, D.; Kopecek, J.; Kissel, T. *Pharm. Res.* **2002**, *19*, 140–146.
(30) Bieber, T.; Meissner, W.; Kostin, S.; Niemann, A.; Elsasser, H.-P. *J. Controlled Release* **2002**, *82*, 441–454.
(31) Walker, G. F.; Fella, C.; Pelisek, J.; Fahrmeir, J.; Boeckle, S.; Ogris, M.; Wagner, E. *Mol. Ther.* **2005**, *11*, 418–425.

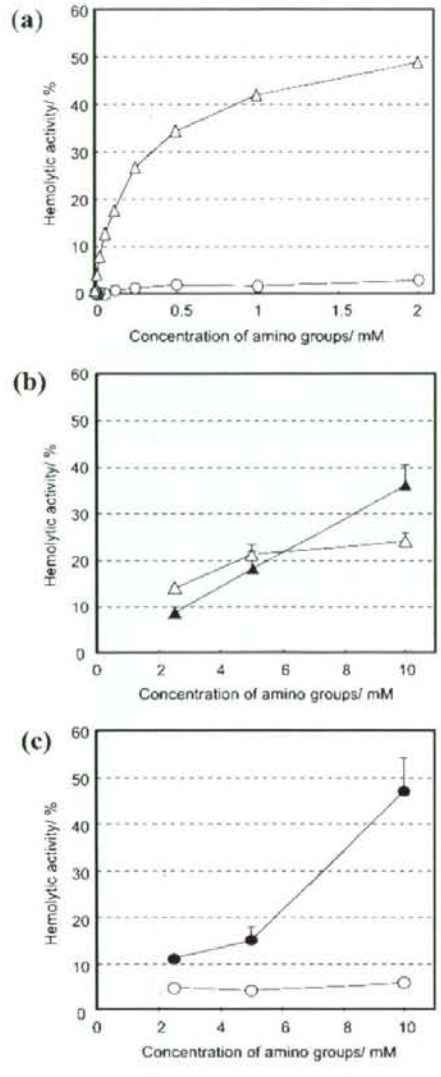

Figure 7. Hemolytic activity of PAsp(DET) and PAsp(DPT) against murine erythrocytes. (a) Hemolytic activity of PAsp(DET) (○) and PAsp(DPT) (△) after overnight erythrocyte incubation at pH 7.4 and 37 °C. (b) Hemolytic activity of PAsp(DPT) after 3 h incubation at pH 7.4 (△) and 5.5 (▲) (at 37 °C). (c) Hemolytic activity of PAsp(DET) after 3 h incubation at pH 7.4 (○) and 5.5 (●) (at 37 °C). Results were expressed as mean ± SEM ($n = 4$).

incubated with RhoB-labeled polycations. Fluorescence from PAsp(DET)−RhoB was not observed at pH 7.4 (Figure 9a) but upon acidic conditions (pH ~5), the fluorescence intensity was significant, extending to the cell periphery (Figure 9b), thereby indicating the appreciable cellular association of PAsp(DET)−RhoB at the acidic pH. In addition, CLSM studies with PAsp(DPT)−RhoB clearly showed significant levels of fluorescence at both pH's (Figure 9c,d), indicating a strong associative behavior of PAsp(DPT)−RhoB to cellular membrane, regardless of the pH. These images are in good agreement with the membrane-destabilizing capacity of the polycations determined by the hemolysis and LDH assays (Figures 7 and 8). It is reasonable to conclude from these results that PAsp-

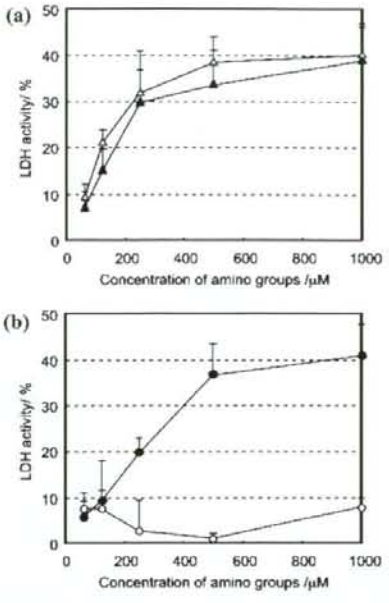

Figure 8. Enzymatic activity of LDH liberated from HUVEC upon interaction with the polycations at 37 °C for 1.5 h. (a) LDH activity for PAsp(DPT) system at pH 7.4 (△) and 5.5 (▲). (b) LDH activity for PAsp(DET) system at pH 7.4 (○) and 5.5 (●). Results were expressed as mean ± SEM ($n = 6$).

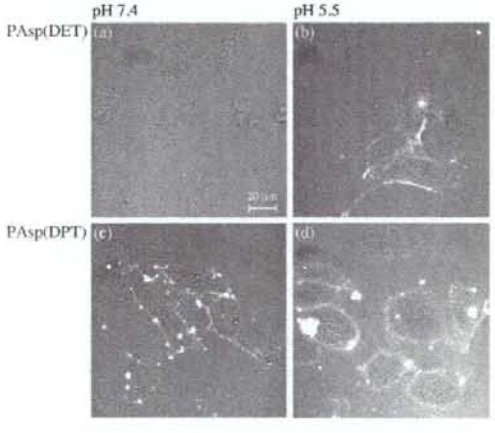

Figure 9. The adsorption of rhodamine B-labeled PAsp(DET) and PAsp(DPT) to HUVEC. The cells were incubated with the RhoB-labeled polycations (brightened as white) at the residual amino group concentration of 100 μM at 4 °C for 1 h, followed by washing with PBS, before CSLM imaging. (a) PAsp(DET) at pH 7.4, (b) PAsp(DET) at pH 5.5, (c) PAsp(DPT) at pH 7.4, (d) PAsp(DPT) at pH 5.5.

(DPT), without high buffering capacity (Figure 1), facilitates endosomal escape of its polyplexes into the cytoplasm through the direct perturbation of endosomal membrane. Nevertheless, the strong capacity of membrane destabilization, even at physiological pH, induces substantial damage to the cell membrane treated with PAsp(DPT) polyplexes as confirmed by the poor cell viability (Figure 5a,b). On the contrary, the weak interaction of PAsp(DET) with the plasma membrane at neutral pH is consistent with the lowered membrane-destabilizing capacity indicated from the results of hemolysis and LDH

assays. These data are supported by the high viability of the cells treated with PAsp(DET) polyplexes, as judged by MTT assay (Figures 5a,b). It should be further emphasized that the cellular association and the membrane-destabilizing capacity of PAsp(DET) were significantly enhanced by decreasing environmental pH to 5.5, becoming comparable to those of PAsp(DPT). This indicates that PAsp(DET) selectively destabilizes the membrane of the endosomal compartment with decreased pH to facilitate the endosomal escape of the polyplexes with minimal damage to the plasma membrane facing an extracellular pH of 7.4. Furthermore, it is reasonable to assume that cytoplasmic PAsp(DET) polyplexes may show minimal interaction with the membranes of organelles because of the pH recovery from acidic to neutral accompanied by the migration from the endosome to cytoplasm. Eventually, PAsp(DET) polyplexes successfully achieved the high transfection efficacy without impairing the cellular viability, as seen in Figure 4.

The unique pH dependency of the affinity of PAsp(DET) to cellular membrane is apparently correlated with the two-step protonation behavior of the flanking 1,2-diaminoethane unit in PAsp(DET). As described in the former section, the 1,2-diaminoethane unit assumes a monoprotonated gauche form at neutral pH, while additional protonation at an acidic pH induces a conformational transition to a diprotonated anti form (Scheme 1). This protonation change accompanying the conformational transition is likely related with the pH-modulated interaction of PAsp(DET) with the cellular membrane. Apparently, PAsp(DET) with the diamine unit in the monoprotonated gauche state exhibited a weak affinity for the cellular membrane but the diprotonated anti state revealed an increased affinity to perturb the membrane integrity. In contrast, the 1,3-diaminopropane unit in PAsp(DPT) assumes a diprotonated form at physiological, late endosomal, and lysosomal pH conditions; moreover, PAsp(DPT) shows a strong interaction with the cellular membrane, even at neutral pH conditions.

Conclusion

The present study was devoted to clarify key chemical parameters for the next generation of polycation/polyplexes exhibiting augmented levels of transfection efficacy and negligible cytotoxicity both in vitro and in vivo. This work primarily focused on N-substituted cationic poly(aspartamide) derivatives, PAsp(DET), possessing flanking 1,2-diaminoethane side chain, previously identified for effective in vivo transfection.[15,16] Comparative analysis between PAsp(DET) and PAsp(DPT) revealed that a single methylene unit difference in the diamine side chains had a crucial effect on the multiple cationic charge states. This seemingly minimal chemical change produced a striking contrast in their polyplex transfection behaviors, presumably due to the increased cytotoxicity. The high cytotoxicity of PAsp(DPT) was closely correlated to the degree of membrane destabilization, which was consistent with the strong interaction of PAsp(DPT) with the cellular membrane, even at physiological pH. The results of CLSM, hemolysis, and LDH analysis indicate that the membrane-destabilizing capacity of PAsp(DPT) contributes to the intracellular transport of PAsp(DPT) polyplexes, despite its weak buffering capacity. In contrast, the membrane destabilizing capacity of PAsp(DET) was highly altered, depending on the environmental pH. Two cationic charge states emerged with a monoprotonation at neutral pH and a diprotonated state at acidic conditions. We conclude that PAsp(DET) exhibits pH-selective membrane destabilization for late endosomal or lysosomal escape without compromising the membrane integrity of cytoplasmic vesicles and/or organelles. This unique approach provides the impetus for future nonviral gene vector development from synthetic poly(amino acids) with facile insertion of pH-selective membrane destabilizing structures to augment transfection efficacy and limit cytotoxicity. Thus, we show a novel and effective method to construct smart carrier systems useful for intracellular delivery of versatile bioactive components with inherently poor permeability to cellular membranes.

Acknowledgment. This work was financially supported by the Core Research Program for Evolutional Science and Technology (CREST) from the Japan Science and Technology Corp. (JST) as well as by Special Coordination Funds for Promoting Science and Technology from the Ministry of Education, Culture, Sports, Science and Technology of Japan (MEXT). The authors express their appreciation to Dr. H. Hamada (RIKEN, Japan) for providing the plasmid DNA and Dr. Darin Y Furgeson (University of Wisconsin—Madison) for proofreading of the manuscript. K. Miyata thanks the Research Fellowships of the Japan Society for the Promotion of Science for Young Scientists (JSPS) and the Mitsubishi Chemical Corp. Fund for their financial support.

Supporting Information Available: Experimental Section, Supporting Scheme 1, Supporting Figures 1−4, and Supporting Table 1. This material is available free of charge via the Internet at http://pubs.acs.org.

JA804561G

molecular pharmaceutics

Article

Polyplex Micelles with Cyclic RGD Peptide Ligands and Disulfide Cross-Links Directing to the Enhanced Transfection via Controlled Intracellular Trafficking

Makoto Oba, Kazuhiro Aoyagi, Kanjiro Miyata, Yu Matsumoto, Keiji Itaka, Nobuhiro Nishiyama, Yuichi Yamasaki, Hiroyuki Koyama, and Kazunori Kataoka

Mol. Pharmaceutics, **2008**, 5 (6), 1080-1092 • DOI: 10.1021/mp800070s • Publication Date (Web): 08 October 2008

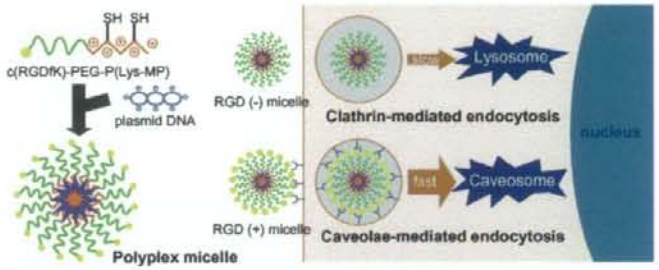

More About This Article

Additional resources and features associated with this article are available within the HTML version:

- Supporting Information
- Access to high resolution figures
- Links to articles and content related to this article
- Copyright permission to reproduce figures and/or text from this article

View the Full Text HTML

articles

molecular pharmaceutics

Polyplex Micelles with Cyclic RGD Peptide Ligands and Disulfide Cross-Links Directing to the Enhanced Transfection via Controlled Intracellular Trafficking

Makoto Oba,[†] Kazuhiro Aoyagi,[‡] Kanjiro Miyata,[§,∥] Yu Matsumoto,[⊥] Keiji Itaka,[⊥] Nobuhiro Nishiyama,[∥,⊥] Yuichi Yamasaki,[‡,∥] Hiroyuki Koyama,[†] and Kazunori Kataoka*[,‡,∥,⊥]

Department of Clinical Vascular Regeneration, Graduate School of Medicine, The University of Tokyo, 7-3-1 Hongo, Bunkyo, Tokyo 113-8655, Japan, Department of Materials Engineering, Graduate School of Engineering, The University of Tokyo, 7-3-1 Hongo, Bunkyo, Tokyo 113-8656, Japan, Center for NanoBio Integration, The University of Tokyo, 7-3-1 Hongo, Bunkyo, Tokyo 113-8656, Japan, Department of Bioengineering, Graduate School of Engineering, The University of Tokyo, 7-3-1 Hongo, Bunkyo, Tokyo 113-8656, Japan, and Center for Disease Biology and Integrative Medicine, Graduate School of Medicine, The University of Tokyo, 7-3-1 Hongo, Bunkyo, Tokyo 113-0033, Japan

Received June 24, 2008; Revised Manuscript Received September 16, 2008; Accepted September 23, 2008

Abstract: Thiolated c(RGDfK)-poly(ethylene glycol)-*block*-poly(lysine) (PEG-PLys), a novel block polymer that has a cyclic RGD peptide in the PEG terminus and thiol groups in the PLys side chain, was prepared and applied to the preparation of targetable disulfide cross-linked polyplex micelles through ion complexation with plasmid DNA (pDNA). The obtained polyplex micelles achieved remarkably enhanced transfection efficiency against cultured HeLa cells possessing $\alpha_v\beta_3$ integrin receptors, which are selectively recognized by cyclic RGD peptides, demonstrating the synergistic effect of cyclic RGD peptide ligands on the micelle surface and disulfide cross-links in the core to exert the smooth release of pDNA in the intracellular environment via reductive cleavage. This enhancement was not due to an increase in the uptake amount of polyplex micelles but to a change in their intracellular trafficking route. Detailed confocal laser scanning microscopic observation revealed that polyplex micelles with cyclic RGD peptide ligands were distributed in the perinuclear region in the early stages preferentially through caveolae-mediated endocytosis, which may be a desirable pathway for avoiding the lysosomal degradation of delivered genes. Hence, this approach to introducing ligands and cross-links into the polyplex micelles is promising for the construction of nonviral gene vectors that enhance transfection by controlling intracellular distribution.

Keywords: Polymeric micelle; cyclic RGD peptide; disulfide cross-links; caveolae-mediated endocytosis

Introduction

As an alternative to viral gene vectors with intrinsic safety issues, there is a growing demand for nonviral gene vectors.[1,2] Despite this demand, nonviral gene vectors based on cationic lipids (lipoplexes) and cationic polymers (polyplexes) are still insufficiently for *in vivo* applications, particularly those administered systemically. To achieve

* To whom correspondence should be addressed. Mailing address: The University of Tokyo, Department of Materials Engineering, 7-3-1 Hongo, Bunkyo-ku, Tokyo, 113-8656, Japan. Tel: +81-3-5841-7138. Fax: +81-3-5841-7139. E-mail: kataoka@bmw.t.u-tokyo.ac.jp.

† Department of Clinical Vascular Regeneration, Graduate School of Medicine.

‡ Department of Materials Engineering, Graduate School of Engineering.

§ Department of Bioengineering, Graduate School of Engineering.

∥ Center for NanoBio Integration.

⊥ Center for Disease Biology and Integrative Medicine, Graduate School of Medicine.

10.1021/mp800070s CCC: $40.75
Published on Web 10/08/2008

sufficient *in vivo* systemic transfection, nonviral vectors need to satisfy several properties, such as high stability in the bloodstream, accumulation in target tissues, and controlled intracellular trafficking directing to the nucleus.

Polyplex micelles, composed of poly(ethylene glycol) (PEG)-polycation block copolymers and plasmid DNA (pDNA), are nonviral gene vectors with the potential for systemic application,[3−5] because of the suitable size of approximately 100 nm for systemic administration, and the formation of the biocompatible PEG shell layer to avoid the nonspecific interaction with blood components.[6−8] To further improve the stability and transfection efficiency of polyplex micelles, disulfide cross-links were introduced into the micelle core, revealing the improved transfection to cultured cells as well as the successful reporter gene expression in mouse liver by systemic administration.[9,10] Furthermore, we recently established a procedure to install cyclic RGD peptide ligands (c(RGDfK)), which can selectively recognize $\alpha_v\beta_3$ and $\alpha_v\beta_5$ integrin receptors, on the surface of a polyplex micelle. Eventually, c(RGDfK) installed polyplex micelles exhibited enhanced transfection efficiency against specific cells possessing $\alpha_v\beta_3$ and $\alpha_v\beta_5$ integrin receptors, such as HeLa cells.[11] $\alpha_v\beta_3$ integrin receptors are known to be overexpressed in endothelial cells of tumor capillaries and neointimal tissues. It should be noted that the use of vectors with cyclic RGD peptide ligands has been investigated as an active targeting strategy in antiangiogenic gene therapy for cancer.[12−14] Nevertheless, those studies focused primarily on therapeutic through the facilitation of cellular uptake of the vectors through receptor-mediated routes, and less attention has been paid to the intracellular trafficking of the vectors possibly modulated by the installed ligands. Worth mentioning in this regard is our previous finding that installation of cyclic RGD ligands on the polyplex micelle surface facilitated their localization in the perinuclear region, suggesting the modulated trafficking induced by cyclic RGD ligands.[11]

The study reported here is devoted to get further insights into the modulated cellular uptake and subsequent trafficking of c(RGDfK) installed polyplex micelles in order to enhance transfection efficiency. For this purpose, new polyplex micelles with integrated functions were developed by installing cyclic RGD ligands on the surface and disulfide cross-links in the core. Indeed, the PEG-*block*-poly(lysine) (PEG-PLys) block copolymer as a platform polymer was modified by introducing a cyclic RGD peptide into the PEG terminus as well as thiol groups into the side chain of the PLys segment. The functions of prepared polyplex micelles were tested against HeLa cells possessing $\alpha_v\beta_3$ and $\alpha_v\beta_5$ integrin receptors; the transfection efficiency, the amount of cellular uptake, and the intracellular distribution were thus determined. In particular, the intracellular trafficking of the polyplex micelles loaded with Cy3- or Cy5-labeled pDNA was evaluated thoroughly by confocal laser scanning microscope (CLSM) observation, which clarified the uptake route and the final intracellular localization. The results demonstrated that cyclic RGD ligands facilitated the caveolae-mediated endocytosis of the polyplex micelles and thus improved transfection efficiency, which is apparently important for the design of nonviral gene vectors that can avoid lysosomal degradation. Moreover, cyclic RGD ligands should

(1) Pack, D. W.; Hoffman, A. S.; Pun, S.; Stayton, P. S. Design and Development of Polymers for Gene Delivery. *Nat. Rev. Drug Discovery* **2005**, *4*, 581–593.

(2) Mastrobattista, E.; van der Aa, M. A.; Hennink, W. E.; Crommelin, D. J. A. Artificial Viruses: a Nanotechnological Approach to Gene Delivery. *Nat. Rev. Drug Discovery* **2006**, *5*, 115–121.

(3) Katayose, S.; Kataoka, K. Water-Soluble Polyion Complex Associates of DNA and Poly(ethylene glycol)-Poly(L-lysine) Block Copolymer. *Bioconjugate Chem.* **1997**, *8*, 702–707.

(4) Kakizawa, Y.; Kataoka, K. Block Copolymer Micelles for Delivery of Gene and Related Compounds. *Adv. Drug Delivery Rev.* **2002**, *54*, 203–222.

(5) Osada, K.; Kataoka, K. Drug and Gene Delivery Based on Supramolecular Assembly of PEG-Polypeptide Hybrid Block Copolymers. *Adv. Polym. Sci.* **2006**, *202*, 113–153.

(6) Itaka, K.; Yamauchi, K.; Harada, A.; Nakamura, K.; Kawaguchi, H.; Kataoka, K. Polyion Complex Micelles from Plasmid DNA and Poly(ethylene glycol)-Poly(L-lysine) Block Copolymer as Serum-Tolerable Polyplex System: Physicochemical Properties of Micelles Relevant to Gene Transfection Efficiency. *Biomaterials* **2003**, *24*, 4495–4506.

(7) Han, M.; Bae, Y.; Nishiyama, N.; Miyata, K.; Oba, M.; Kataoka, K. Transfection Study Using Multicellular Tumor Spheroids for Screening Non-Viral Polymeric Gene Vectors with Low Cytotoxicity and High Transfection Efficiencies. *J. Controlled Release* **2007**, *121*, 38–48.

(8) Akagi, D.; Oba, M.; Koyama, H.; Nishiyama, N.; Fukushima, S.; Miyata, T.; Nagawa, H.; Kataoka, K. Biocompatible Micellar Nanovectors Achieve Efficient Gene Transfer to Vascular Lesions without Cytotoxicity and Thrombus Formation. *Gene Ther.* **2007**, *14*, 1029–1038.

(9) Miyata, K.; Kakizawa, Y.; Nishiyama, N.; Harada, A.; Yamasaki, Y.; Koyama, H.; Kataoka, K. Block Catiomer Polyplexes with Regulated Densities of Charge and Disulfide Cross-Linking Directed to Enhanced Gene Expression. *J. Am. Chem. Soc.* **2004**, *126*, 2355–2361.

(10) Miyata, K.; Kakizawa, Y.; Nishiyama, N.; Yamasaki, Y.; Watanabe, T.; Kohara, M.; Kataoka, K. Freeze-Dried Formulations for In Vivo Gene Delivery of PEGylated Polyplex Micelles with Disulfide Crosslinked Cores to the Liver. *J. Controlled Release* **2005**, *109*, 15–23.

(11) Oba, M.; Fukushima, S.; Kanayama, N.; Aoyagi, K.; Nishiyama, N.; Koyama, H.; Kataoka, K. Cyclic RGD Peptide-Conjugated Polyplex Micelles as a Targetable Gene Delivery System Directed to Cells Possessing $\alpha_v\beta_3$ and $\alpha_v\beta_5$ Integrins. *Bioconjugate Chem.* **2007**, *18*, 1415–1423.

(12) Kim, W. J.; Yockman, J. W.; Lee, M.; Jeong, J. H.; Kim, Y. H.; Kim, S. W. Soluble *Flt-1* Gene Delivery Using PEI-*g*-PEG-RGD Conjugate for Anti-Angiogenesis. *J. Controlled Release* **2005**, *106*, 224–234.

(13) Kim, W. J.; Yockman, J. W.; Jeong, J. H.; Christensen, L. V.; Lee, M.; Kim, Y. H.; Kim, S. W. Anti-Angiogenic Inhibition of Tumor Growth by Systemic Delivery of PEI-*g*-PEG-RGD/pCMV-sFlt-1 Complexes in Tumor-Bearing Mice. *J. Controlled Release* **2006**, *114*, 381–388.

(14) Schiffelers, R. M.; Ansari, A.; Xu, J.; Zhou, Q.; Tang, Q.; Storm, G.; Molema, G.; Lu, P. Y.; Scaria, P. V.; Woodle, M. C. Cancer siRNA Therapy by Tumor Selective Delivery with Ligand-Targeted Sterically Stabilized Nanoparticle. *Nucleic Acids Res.* **2004**, *32*, e149.

eventually achieve appreciable transfection efficiency even for systems without high endosomal-disrupting properties, including PLys-based polyplex systems.

Experimental Section

Materials. *N,N*-Diisopropylethylamine (DIEA), dithiothreitol (DTT), aphidicolin, and D-luciferin were purchased from Wako Pure Chemical Industries (Osaka, Japan). *N*-Methyl-2-pyrrolidone (NMP) was purchased from Aldrich Chemical (Milwaukee, WI). *N*-Succinimidyl 3-(2-pyridyldithio)-propionate (SPDP) was purchased from Dojindo Laboratories (Kumamoto, Japan). Cyclo[RGDfK(CX-)] (c(RGDfK)) peptides (X = 6-aminocaproic acid: ε-Acp) was purchased from Peptide Institute (Osaka, Japan). Acetal-poly(ethylene glycol)-*block*-poly(lysine) (acetal-PEG-PLys) and c(RGDfK)-PEG-PLys block copolymers (PEG, 12 000 g/mol; polymerization degree of PLys segment, 72; introduction rate of c(RGDfK) peptide, 66%) were synthesized as previously reported.[11] A micro-BCA protein assay reagent kit was purchased from Pierce Chemical (Rockford, IL). The luciferase assay kit was a product of Promega (Madison, WI). Plasmid pCAcc+Luc coding for firefly luciferase under the control of the CAG promoter was provided by RIKEN Gene Bank (Tsukuba, Japan), amplified in competent DH5α *Escherichia coli*, and then purified using a HiSpeed Plasmid MaxiKit purchased from Qiagen Sciences (Germantown, MD).

Synthesis of Block Copolymers: (a) Acetal-poly(ethylene glycol)-block-poly[ε-3-(2-pyridyldithio)propionyl lysine] (Acetal-PEG-P(Lys-PDP)). Pyridyldithiopropionyl (PDP) groups were introduced to the PLys side chain by the use of a heterobifunctional reagent, SPDP. The typical synthesis procedure is described as follows for the acetal-PEG-P(Lys-PDP) (5 mol % PDP): Acetal-PEG-PLys (200 mg, 8.38 μmol) and SPDP (11.7 mg, 37.7 μmol) were separately dissolved in NMP containing 5 wt % LiCl (10 mL for acetal-PEG-PLys, 1 mL for SPDP). A solution containing SPDP and DIEA (1.05 mL, 377 μmol) was added to acetal-PEG-PLys solution and stirred at room temperature for 3 h. The mixture was then precipitated into an approximately 20-times-excess volume of diethyl ether. The polymer was dissolved in 10 mM phosphate buffer (pH 7.0) with 150 mM NaCl, dialyzed against the same buffer solution and distilled water, and lyophilized to obtain acetal-PEG-P(Lys-PDP) (166 mg, 80%).

(b) c(RGDfK)-poly(ethylene glycol)-block-poly[ε-(3-mercaptopropinonyl) lysine] (c(RGDfK)-PEG-P(Lys-MP)). The typical synthesis procedure is described as follows for the c(RGDfK)-PEG-P(Lys-MP) (5 mol % MP): Acetal-PEG-P(Lys-PDP) (30 mg, 1.21 μmol) was dissolved in 10 mM Tris-HCl buffer solution (pH 7.4) (3 mL) with DTT (6.76 mg, 43.9 μmol). After 30 min incubation at room temperature, the polymer solution was dialyzed against 0.2 M AcOH buffer (pH 4.0). c[RGDfK(CX-)] (10.4 mg, 12.8 mmol) in AcOH buffer (3 mL) was then added to the polymer solution. After stirring for 5 days, DTT (6.67 mg, 43.9 μmol) was added and stirred at room temperature for 3 h. The reacted polymer was purified by dialysis sequentially against 10 mM phosphate buffer (pH 7.0) with 150 mM NaCl and distilled water, and lyophilized to obtain c(RGDfK)-PEG-P(Lys-MP) (20.5 mg, 71%).

The ^{1}H NMR spectrum of each polymer was obtained with an EX300 spectrometer (JEOL, Tokyo, Japan). Chemical shifts were reported in ppm relative to the residual protonated solvent resonance. Block copolymer with X% of thiolation degree was abbreviated as B-SHX%.

Preparation of Polyplex Micelles. Each thiolated block copolymer was dissolved in 10 mM Tris-HCl buffer (pH 7.4), followed by the addition of 3-times-excess mol of DTT against the PDP or MP group. After 30 min incubation at room temperature, the polymer solution in varying concentrations was added to a twice-excess volume of 50 μg/mL pDNA/10 mM Tris-HCl (pH 7.4) solution to form polyplex micelles with different compositions. The final pDNA concentration was adjusted to 33.3 μg/mL. The N/P ratio was defined as the residual molar ratio of amino groups of PLys to the phosphate groups of pDNA. After overnight incubation at room temperature, the polyplex micelle solution was dialyzed against 10 mM Tris-HCl (pH 7.4) containing 0.5 vol% DMSO at 37 °C for 24 h to remove the impurities, followed by 2 days of additional dialysis to remove DMSO. During the dialysis, the thiol groups of thiolated block copolymers were oxidized to form disulfide cross-links. To follow the oxidation process, the remaining thiol groups in disulfide cross-linked micelles were determined by Ellman's method.[15] Polyplex micelles with and without cyclic RGD peptide ligands were abbreviated as RGD (+) and RGD (−) micelles, respectively.

Dynamic Light Scattering Measurement. The sizes of the polyplex micelles were evaluated by dynamic light scattering (DLS) using the Nano ZS zetasizer (ZEN3600, Malvern Instruments, Worcestershire, U.K.). A He−Ne ion laser (633 nm) was used for the incident beam. Polyplex micelle solutions (33.3 μg pDNA/mL) with an N/P = 2 in 10 mM Tris-HCl (pH 7.4) were used for the measurements. The data obtained at a detection angle of 173 ° and a temperature of 25 °C were analyzed by a cumulant method to obtain the hydrodynamic diameters and polydispersity indices (μ/Γ^2) of the micelles. The results reported were expressed as mean values (± SEM) of four experiments.

ζ-Potential Measurement. The ζ-potentials of the polyplex micelles were evaluated by the laser-doppler electrophoresis method using Nano ZS with a He−Ne ion laser (633 nm). Polyplex micelle solution with an N/P = 2 was adjusted to a concentration of 20 μg pDNA/mL. The ζ-potential was measured at 25 °C. A scattering angle of 173 ° was used in these measurements. The results were expressed as the mean values (± SEM) of four experiments.

Atomic Force Microscopy (AFM) Imaging. Five microliters of each sample was deposited on a freshly cleaved

(15) Riddles, P. W.; Blakeley, R. L.; Zerner, B. Ellman's Reagent: 5,5′-Dithiobis(2-nitrobenzoic Acid)- a Reexamination. *Anal. Biochem.* **1979**, *94*, 75–81.

Scheme 1. Synthesis Route of c(RGDfK)-PEG-P(Lys-MP) Block Copolymer

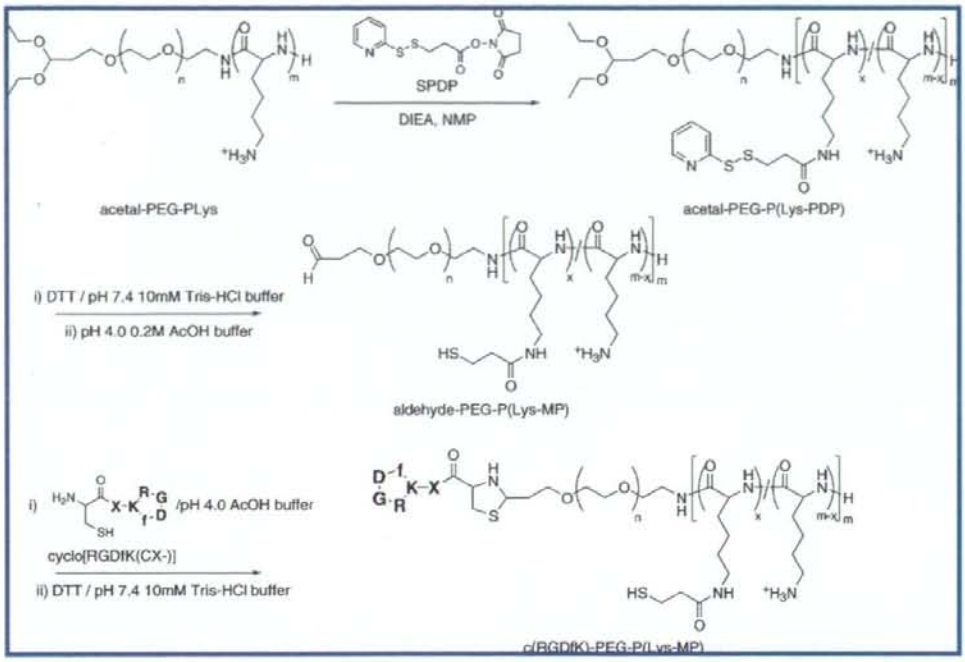

mica substrate for 30 s and then adequately dried under a gentle flow of nitrogen gas. AFM imaging was performed in a tapping mode with MPP-11100 (Vecco Instruments, Woodbury, NY) on a Nano Scope (Vecco Instruments) operated by Nanoscope IIIa software (Digital Instruments, Santa Barbara, CA). The cantilever oscillation frequency was

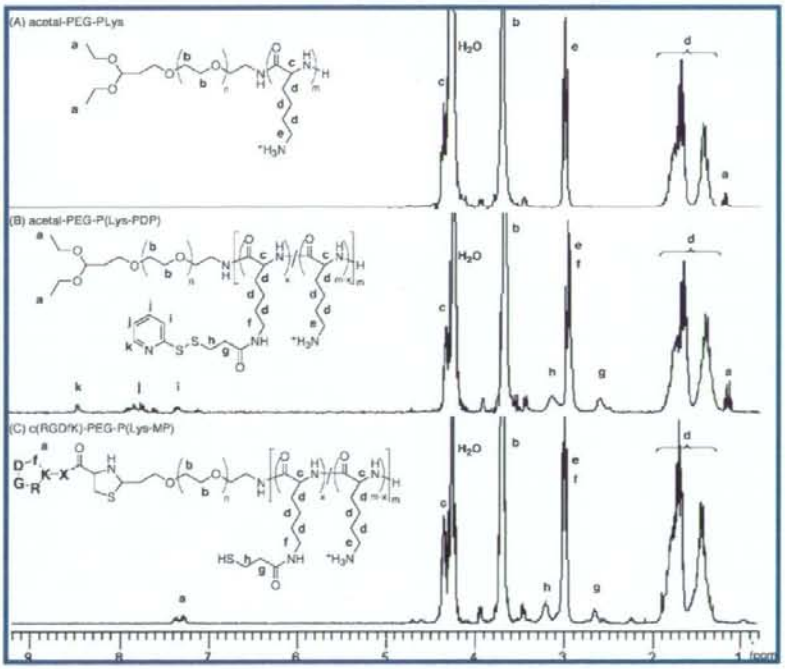

Figure 1. ^{1}H NMR spectra of acetal-PEG-PLys (A), acetal-PEG-P(Lys-PDP) (B-SH5%) (B), and c(RGDfK)-PEG-P-(Lys-MP) (B-SH5%) (C) in D_2O at 80 °C.

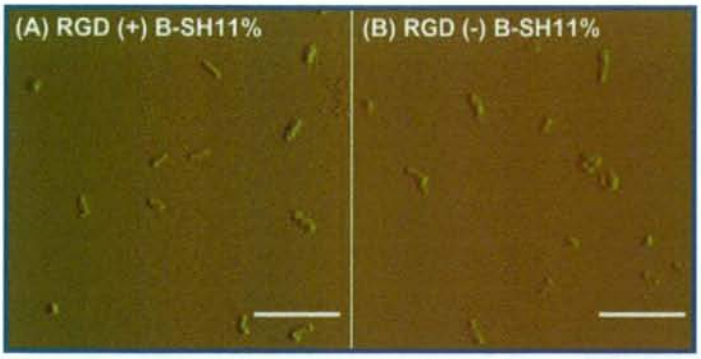

Figure 2. AFM images of cross-linked micelles (B-SH11%, N/P = 2) with (A) or without (B) cyclic RGD peptide ligands. The scale bars represent 500 nm.

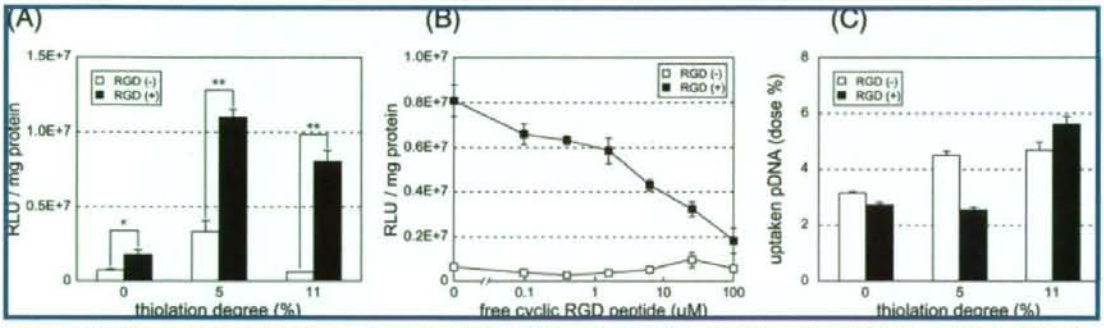

Figure 3. In vitro transfection efficiency and cellular uptake of polyplex micelles against HeLa cells. (A) Effects of cyclic RGD peptide ligands on transfection efficiency for micelles with varying thiolation degrees (N/P = 2). (B) Inhibitory effect of free cyclic RGD peptide on the transfection with B-SH11% polyplex micelles (N/P = 2) with or without cyclic RGD peptide ligands. (C) Cellular uptake of RGD (+) and RGD (−) polyplex micelles (N/P = 2) loading ^{32}P-labeled pDNA. Error bars in the graphs represent SEM, $n = 4$. $P^* < 0.05$ and $P^{**} < 0.01$.

tuned to the resonance frequency of the cantilever, 260−340 kHz. The images were recorded at a 2 μm/s linear scanning speed and with a sampling density of 61 nm^2 per pixel. Raw AFM images were processed only by background removal (flattening) using a microscope manufacturer's image-processing software.

Transfection. HeLa cells were seeded on 24-well culture plates (10 000 cells/well) and incubated overnight in 500 μL of Dulbecco's modified Eagle's medium (DMEM) containing 10% fetal bovine serum (FBS). The medium was replaced with fresh medium, after which polyplex solution (N/P = 2) was applied to each well (1 μg of pDNA/well). After 24 h incubation, the medium was replaced with 500 μL of fresh medium, followed by 24 h reincubation. The luciferase gene expression was then evaluated based on the intensity of photoluminescence intensity using the Luciferase assay kit and a Lumat LB9507 luminometer (Berthold Technologies, Bad Wildbad, Germany). The amount of protein in each well was concomitantly determined using a Micro BCA protein assay reagent kit.

Inhibitory Effect of Free Cyclic RGD Peptides. HeLa cells were seeded on 24-well culture plates (10 000 cells/well) and incubated overnight in 500 μL of DMEM containing 10% FBS. The medium was replaced with fresh medium containing various concentrations of cyclo[RGDfK(CX-)], followed by 3 h incubation. The polyplex micelle solution (B-SH11%, N/P = 2) was applied to each well (1 μg pDNA/well). After 24 h incubation, the medium was replaced with 500 μL of fresh medium, followed by 24 h reincubation. The luciferase gene expression was then evaluated in the same way as described in the Transfection section.

Analysis of Cellular Uptake of Polyplex Micelles. pDNA was radioactively labeled by incorporation of ^{32}P-dCTP (GE Healthcare U.K., Buckinghamshire, U.K.) using a nick translation system (Invitrogen, Carlsbad, CA) according to the manufacturer's protocol. Unincorporated nucleotides were carefully removed using the High Pure PCR Product Purification Kit (Roche, Basel, Switzerland). HeLa cells were seeded on 24-well culture plates (10 000 cells/well) and incubated overnight in 500 μL of DMEM containing 10% FBS. The medium was replaced with fresh medium, after which the polyplex micelle incorporating the mixture of nonlabeled and ^{32}P-labeled pDNA (N/P = 2) was applied to each well (1 μg pDNA/well). After 24 h incubation, the medium was removed and the cells were washed 3 times with PBS. The cells were lysed with 400 μL of cell culture lysis reagent (Promega) for 30 min at room temperature, after which the lysate was mixed with 5 mL of Ultima Gold

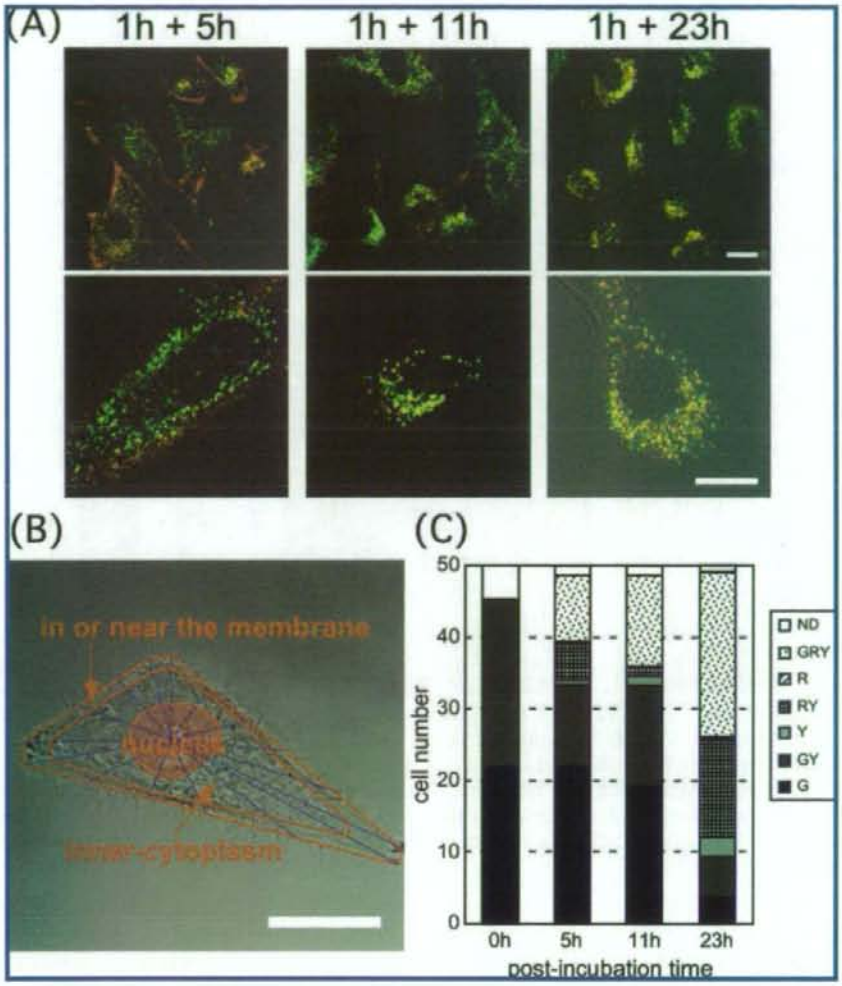

Figure 4. Intracellular distribution B-SH11% polyplex micelles (N/P = 2). RGD (−) micelles loading Cy5-labeled pDNA (red) and RGD (+) micelles loading Cy3-labeled pDNA (green) were simultaneously added and incubated with HeLa cells for 1 h. After replacement with fresh medium, cells were reincubated for the indicated reincubation times (5 h, 11 h, 23 h). (A) CLSM images. Scale bars represent 20 μm. (B) Definitions of "nucleus", "inner-cytoplasm", and "in or near the membrane" regions. "Inner-cytoplasm" was defined as three-quarters of the area from the nucleus to the cell membrane, and "in or near the membrane" was defined as the remaining quarter on the side of the cell membrane. (C) Quantitative analysis of the inner-cytoplasmic distribution of pDNA transfected by polyplex micelles with or without RGD ligands. Fifty different cells were observed and evaluated for each time point. G: green (Cy3-labeled pDNA loaded in RGD (+) micelles). R: red (Cy5-labeled pDNA loaded in RGD (−) micelles). Y: yellow (colocalized Cy3-labeled and Cy5-labeled pDNAs). ND: not detectable (no colors detectable from pDNA).

(Perkin-Elmer, Waltham, MA). Measurements were performed using the Tricarb 2200CA liquid scintillation analyzer (Packard, Meriden, CT) with a counting time of 1 min. The amounts of uptaken pDNA were calculated using a standard curve calibrated with naked ^{32}P-labeled pDNA.

CLSM Observation. pDNA was labeled with Cy3 or Cy5 according to the manufacturer's protocol. Briefly, pDNA was labeled using the Label IT Nucleic Acid Labeling Kit (Mirus, Madison, WI). HeLa cells (30 000 cells) were seeded on a 35 mm glass base dish (Iwaki, Tokyo, Japan) and incubated overnight in 1 mL of DMEM containing 10% FBS, followed by replacement with fresh medium. In the simultaneous observation of RGD (−) and RGD (+) micelles (Figure 4), RGD (−) B-SH11% polyplex micelle solution containing 3 μg Cy5-labeled pDNA (N/P = 2) and RGD (+) B-SH11% polyplex micelle solution containing 3 μg Cy3-labeled pDNA (N/P = 2) were simultaneously applied to a glass dish with cultured HeLa cells. The measurement condition was adjusted so as to obtain almost the same fluorescence intensities between RGD (+) B-SH11% micelles containing Cy3-

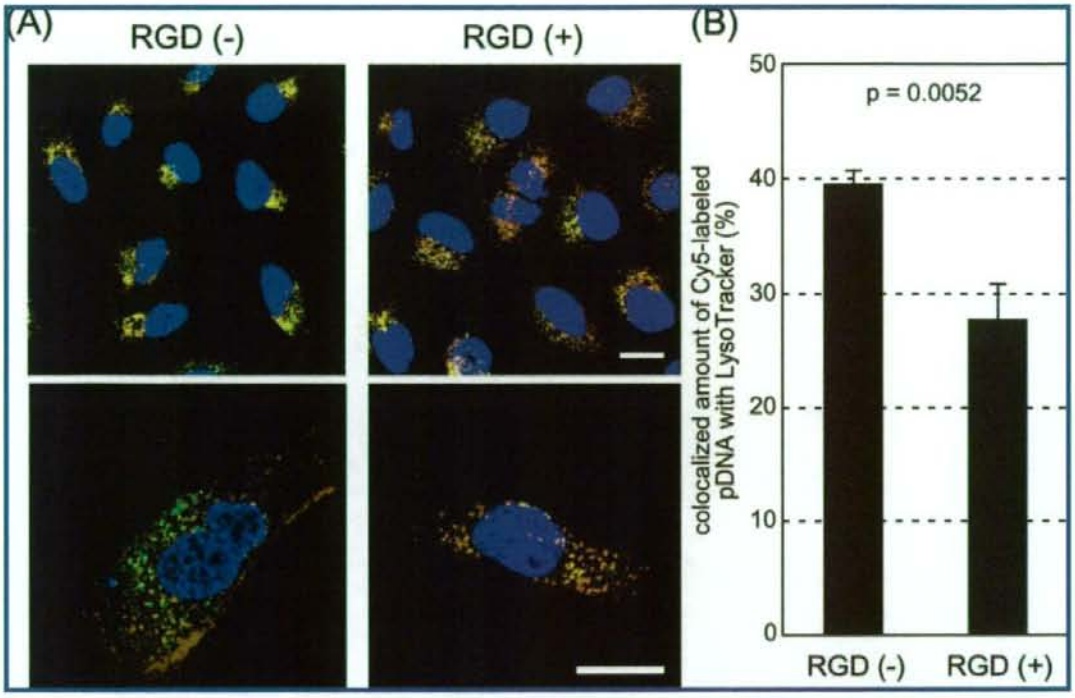

Figure 5. Distribution of RGD (+) and RGD (−) B-SH11% polyplex micelles (N/P = 2) in late endosomes and lysosomes. Polyplex micelles loading Cy5-labeled pDNA (red) were incubated with HeLa cells for 1 h. After replacement with fresh medium, the cells were reincubated for 11 h. The cell nuclei were stained with Hoechst 33342 (blue), and the acidic late endosomes and lysosomes were stained with LysoTracker Green (green). (A) CLSM images of the cells transfected with RGD (−) micelles (left) and RGD (+) micelles (right). The scale bars represent 20 μm. (B) Quantification of Cy5-labeled pDNA colocalized with LysoTracker Green in the inner-cytoplasm. Error bars in the graph represent SEM (n = 10).

labeled pDNA and RGD (+) B-SH11% micelles containing Cy5-labeled pDNA. In the observation with organelle staining (Figures 5 and 6), either RGD (−) or RGD (+) B-SH11% polyplex micelle solution containing Cy5-labeled pDNA (N/P = 2) was applied to a dish with cultured HeLa cells. After various incubation periods, the medium was removed and the cells were washed 3 times with PBS. The intracellular distribution of the polyplex micelles was observed by CLSM after staining acidic late endosomes and lysosomes with LysoTracker Green (Molecular Probes, Eugene, OR), lipid rafts and caveosomes with cholera toxin subunit B (CT-B) Alexa Fluor 488 conjugate (Molecular Probes), and the nuclei with Hoechst 33342 (Dojindo Laboratories, Kumamoto, Japan). The CLSM observation was performed using an LSM 510 (Carl Zeiss, Oberlochen, Germany) with a C-Apochromat 63X objective (Carl Zeiss) at the excitation wavelength of 488 nm (Ar laser) for LysoTracker Green and CT-B Alexa Fluor 488, 543 nm (He−Ne laser) for Cy3, 633 nm (He−Ne laser) for Cy5, and 710 nm (MaiTai laser, two photon excitation; Spectra-Physics, Mountain View, CA) for Hoechst 33342, respectively.

Evaluation of Intracellular Distribution of Polyplex Micelles. To evaluate the amounts of polyplex micelles in cytoplasm, polyplex micelles internalized into the inner region of the cytoplasm were distinguished from polyplex micelles adsorbing onto the cell membrane by reference to a previous paper,[16] in which the cytoplasm was divided into four quadrants to study the intracellular spatial variation of polyplexes (Figure 4B). First, an intracellular region was divided into three areas: "nucleus", "inner-cytoplasm", and "in or near the membrane". "Inner-cytoplasm" was defined as a three-quarters of the area from the nucleus to the cell membrane, and "in or near the membrane" was defined as remaining quarter area on the side of the cell membrane, as illustrated in Figure 4B. From the observation of 50 different cells, the relative amounts of RGD (−) micelles (red) and RGD (+) micelles (green) in the "inner-cytoplasm" were determined based on the number of cells. The following abbreviations are used in Figure 4C: G, green (Cy3-labeled pDNA); R, red (Cy5-labeled pDNA); Y, yellow (Cy3-labeled pDNA colocalized with Cy5-labeled pDNA); and ND, not detectable (no colors (pDNA) detectable). In brief, GRY represents cells with green, red, and yellow spots indepen-

(16) Suh, J.; Wirtz, D.; Hanes, J. Efficient Active Transport of Gene Nanocarriers to the Cell Nucleus. *Proc. Natl. Acad. Sci. U.S.A.* **2003**, *100*, 3878–3882.

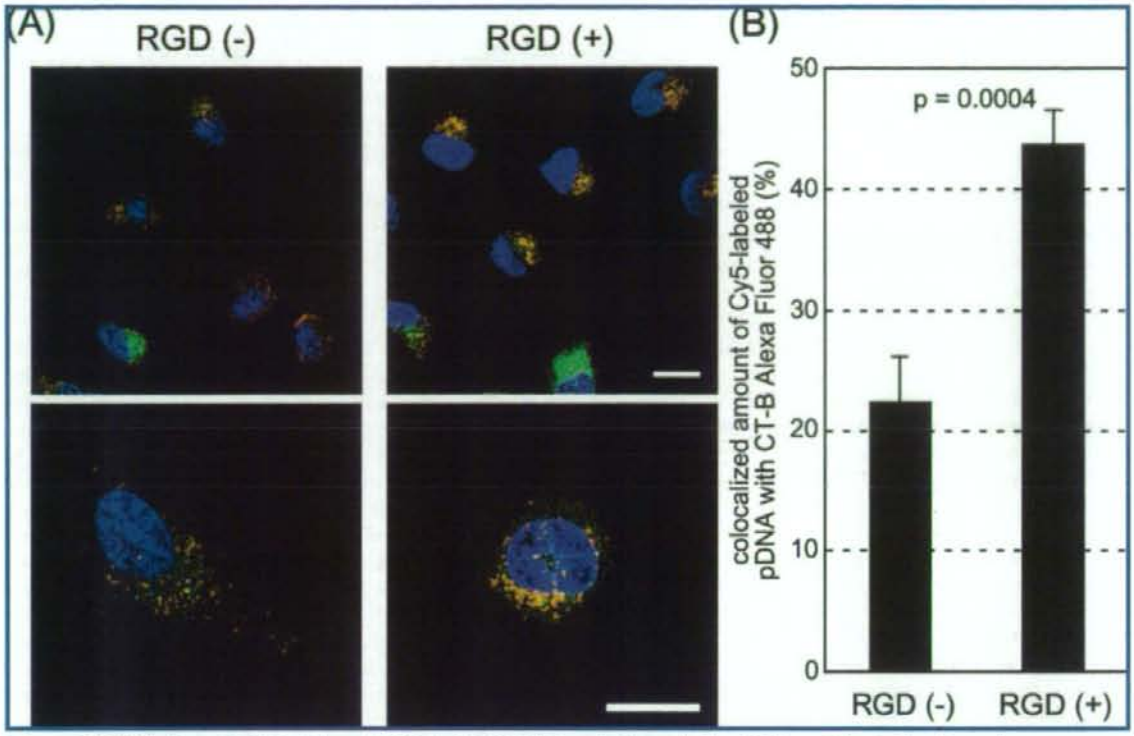

Figure 6. Distribution of RGD (+) and RGD (−) B-SH11% polyplex micelles (N/P = 2) in lipid rafts and caveosomes. Polyplex micelles loading Cy5-labeled pDNA (red) and CT-B Alexa Fluor 488 conjugate (green) were incubated with HeLa cells for 1 h. After replacement with fresh medium, the cells were reincubated for 11 h. The cell nuclei were stained with Hoechst 33342 (blue). (A) CLSM images of RGD (−) micelles (left) and RGD (+) micelles (right). The scale bars represent 20 μm. (B) Quantification of Cy5-labeled pDNA colocalized with CT-B in the inner-cytoplasm. Error bars in the graph represent SEM (n = 10).

dently existing in the "inner-cytoplasm", and GY represents cells with green and yellow spots but without red spots.

To evaluate the final destinations of polyplex micelles, the rate of colocalization of Cy5-labeled pDNA with LysoTracker Green or CT-B Alexa Fluor 488 was quantified (Figures 5B and 6B). LysoTracker Green was used as a marker for the late endosomes and the lysosomes, and CT-B Alexa Fluor 488 was used as a marker for the lipid rafts and the caveosomes. Colocalization was quantified as follows:

$$\text{amount of colocalization (\%)} = \text{Cy5 pixels}_{\text{colocalization}}/\text{Cy5 pixels}_{\text{total}} \times 100$$

where Cy5 $\text{pixels}_{\text{colocalization}}$ represents the number of Cy5 pixels colocalizing with LysoTracker Green or CT-B Alexa Fluor 488 in the inner-cytoplasm, and Cy5 $\text{pixels}_{\text{total}}$ represents the number of all Cy5 pixels in the inner-cytoplasm.

Real-Time Luciferase Gene Expression. HeLa cells (40 000 cells) were seeded on a 35 mm dish (Becton Dickinson, Franklin Lakes, NJ) and incubated overnight in 2 mL of DMEM containing 10% FBS, with or without 10 μg/mL aphidicolin for synchronization of cells. The HeLa cell cycle was arrested in a phase between G1 and S by over 16 h incubation with aphidicolin.[17] The subsequent replacement with fresh medium let cells start to divide at 13 h later. In this assay, three experimental conditions were used to regulate the lag between the time the polyplex micelles were added and the beginning of mitosis. First was the "normal" condition, meaning without any treatments for synchronization. Second was the "3 h mitosis" condition, where each polyplex micelle was added 10 h after the replacement of medium containing aphidicolin with fresh medium, thus setting the start of cell mitosis 3 h after the addition of polyplex micelles. Third was the "13 h mitosis" condition, where each polyplex micelle was added just after the medium replacement, thus commencing cell mitosis 13 h after the addition of the micelles. In the case of the "normal" and "13 h mitosis" conditions, after replacement with fresh medium containing 0.1 mM D-luciferin, RGD (−) or RGD (+) B-SH11% polyplex micelles (N/P = 2) containing 3 μg of pDNA were immediately added. In the case of the "3 h

(17) Pedrali-Noy, G.; Spadari, S.; Miller-Faures, A.; Miller, A. O. A.; Kruppa, J.; Koch, G. Synchronization of HeLa Cell Cultures by Inhibition of DNA Polymerase α with Aphidicolin. *Nucleic Acids Res.* **1980**, *8*, 377–387.

mitosis" condition, polyplex micelles were added 10 h after the replacement with fresh medium containing 0.1 mM D-luciferin. The dishes were set in a luminometer incorporated in a CO_2 incubator (AB-2550 Kronos Dio, ATTO, Tokyo, Japan), and the bioluminescence was monitored every 20 min with an exposure time of 2 min.

Results

Synthesis of c(RGDfK)-PEG-P(Lys-MP). (Scheme 1). Thiolation of acetal-PEG-PLys block copolymer was carried out using a previously described method.[9] Briefly, SPDP was used as a thiolating reagent and reacted with ε-amino group of Lys unit; consequently, a 3-(2-pyridyldithio)propionyl (PDP) group was introduced via an amide bond. Note that the introduction of the thiol group by SPDP decreased the cationic charge density of the PLys segment as the introduction rate increased. Thiolated acetal-PEG-P(Lys-PDP) block copolymers with two types of thiolation degree, 5.04% (B-SH5%) and 10.5% (B-SH11%), were prepared. The PDP introduction rates were calculated from the peak intensity ratio of the methylene protons of PEG (OCH_2CH_2, $\delta = 3.7$ ppm) to the pyridyl protons of the PDP group (C_5H_4N, $\delta =$ 7.0−8.5 ppm) measured by ^1H NMR as typically seen in Figure 1B (B-SH5%).

Conjugation of c(RGDfK) peptide ligands into the PEG terminus of acetal-PEG-P(Lys-PDP) was achieved through the formation of a thiazolidine ring between an N-terminal cysteine and an aldehyde group converted from the acetal group.[11] The acetal group was deprotected under moderate acidic conditions to the aldehyde group. To avoid an exchange reaction between the thiol group of cysteine residue in the c(RGDfK) peptide and the pyridylthio group in the acetal-PEG-P(Lys-PDP), the pyridylthio group was deprotected with DTT prior to the installation of the ligand. After the dialysis against the AcOH buffer to remove excessive DTT as well as to convert the acetal group to an aldehyde group, the c(RGDfK) peptide was added to react with the aldehyde-PEG-P(Lys-MP) in AcOH buffer, resulting in the introduction of the peptide ligand. This type of conjugation between the N-terminal cysteine and the aldehyde group occurs selectively even in the presence of primary amines, since the conjugation through a Schiff base between a primary amine and the aldehyde group is reversible, whereas the conjugation through a thiazolidine ring between the N-terminal cysteine and the aldehyde group is irreversible. The methyl protons of the acetal group ($\delta = 1.2$ ppm) and the aromatic protons of the pyridylthio group ($\delta = 7.0$−8.5 ppm) completely disappeared with the appearance of protons assigned to the aromatic ring of D-phenylalanine (f: D-Phe) ($\delta = 7.3$ and 7.4 ppm) in the c(RGDfK) (Figure 1C). Based on the peak intensity ratios of the aromatic protons of the peptide ligands to the methylene protons of PEG ($\delta = 3.7$ ppm), the introduction rates of the peptide ligands in the c(RGDfK)-PEG-P(Lys-MP) were determined to be 73% and 87% for the B-SH5% and the B-SH11%, respectively.

Formation of Polyplex Micelles. Agarose gel electrophoresis showed that free pDNA was not detected in the polyplex micelles at N/P = 2 (data not shown), confirming that all of the pDNA were entrapped in polyplex micelles. Ellman's test revealed that less than 2% of the thiol groups in the polyplex micelles were free (data not shown), suggesting that almost all of the thiol groups seem to be involved in the formation of disulfide bonds. These results are consistent with our previous report.[9] The sizes, shapes, and ζ-potentials of the cross-linked polyplex micelles were evaluated by DLS, AFM, and laser-doppler electrophoresis, respectively. Table 1 summarizes the cumulant diameters and ζ-potentials of the polyplex micelles at N/P = 2. The cumulant diameters of all the micelles were approximately 110 nm with a moderate polydispersity index between 0.14 and 0.18, regardless of the composition of the thiolated polymers or the introduction of RGD ligands. Also, the ζ-potentials of all the micelles were kept at slightly positive values between +1.1 and +3.6, which is consistent with the formation of the PEG palisade surrounding the polyplex core.[6,18] Figure 2 shows AFM images of B-SH11% cross-linked micelles with or without RGD ligands, where a toroidal structure in the size range of 60−100 nm and a rodlike structure with a long axis of 160−200 nm were observed, corresponding to the sizes from DLS. These results suggest that the physicochemical characteristics of the polyplex micelles are quite similar regardless of the thiolation degree or the introduction of RGD ligands.

Table 1. Size and ζ-Potential of Polyplex Micelles (N/P = 2) with or without Cyclic RGD Peptide Ligands

thiolation degree (%)	cyclic RGD peptide ligand	cumulant diameter (nm)/ polydispersity index (μ/Γ^2)	ζ-potential (mV)
0	(−)	109 ± 0.75/0.169 ± 0.002	1.47 ± 0.312
	(+)	113 ± 1.11/0.156 ± 0.004	2.27 ± 0.148
5	(−)	115 ± 0.71/0.141 ± 0.007	1.62 ± 0.348
	(+)	106 ± 0.48/0.144 ± 0.009	3.57 ± 0.230
11	(−)	111 ± 0.25/0.145 ± 0.011	1.15 ± 0.788
	(+)	114 ± 1.08/0.172 ± 0.005	1.52 ± 0.213

Transfection. The *in vitro* transfection efficiencies of B-SH0%, B-SH5%, and B-SH11% polyplex micelles with or without RGD ligands were evaluated for HeLa cells possessing $\alpha_v\beta_3$ and $\alpha_v\beta_5$ integrin receptors (Figure 3A). A cyclic RGD peptide is well-known to selectively recognize $\alpha_v\beta_3$ and $\alpha_v\beta_5$ integrins among several integrins.[19] In the transfection experiments with non-cross-linked micelles (B-SH0% micelle), the introduction of RGD ligands led to approximately doubled transfection efficiency. Notably, RGD (+) B-SH5% and RGD (+) B-SH11% micelles with cross-

(18) Harada-Shiba, M.; Yamauchi, K.; Harada, A.; Takamisawa, I.; Shimokado, K.; Kataoka, K. Polyion Complex Micelles as Vectors in Gene Therapy-Pharmacokinetics and In Vivo Gene Transfer. *Gene Ther.* **2002**, *9*, 407–414.

(19) Haubner, R.; Gratias, R.; Difenbach, B.; Goodman, S. L.; Jonczyk, A.; Kessler, H. Structual and Functional Aspects of RGD-Containing Cyclic Pentapeptides as Highly Potent and Selective Integrin $\alpha_v\beta_3$ Antagonists. *J. Am. Chem. Soc.* **1996**, *118*, 7461–7472.

linked cores and RGD ligands showed 10-fold higher efficiency than the ligand-less system without cross-linking (RGD (−) B-SH0% micelle). It is obvious that the effect of ligand installation was drastically enhanced by introducing disulfide cross-linking in the core. RGD (+) B-SH5% polyplex micelles achieved the highest transfection efficiency. Consequently, the combination of core cross-linking and ligand installation enhanced efficiency 20 times more than the polyplex micelles without ligands and cross-links.

Then, to further confirm that the increased transfection efficiency by RGD (+) micelles involves the receptor-mediated mechanism, a competitive assay using free cyclic RGD peptides was carried out for B-SH11% cross-linked micelles (Figure 3B). RGD (+) micelles showed a remarkably high transfection efficiency compared with RGD (−) micelles in the absence of free cyclic RGD peptides ($P < 0.01$). As the concentration of free cyclic RGD peptides increased, the transfection efficiency of RGD (+) micelles accordingly decreased, approaching the transfection level of RGD (−) micelles under the condition of 100 μM cyclic RGD peptides ($P = 0.104$). Thus, the results of the competitive assay indicate that $\alpha_v\beta_3$ and/or $\alpha_v\beta_5$ integrin receptor-mediated endocytosis is involved in the transfection of the RGD (+) micelles against HeLa cells.

Analysis of Cellular Uptake of Polyplex Micelles. In general, the enhanced transfection by ligands has been attributed to an increased uptake of vectors.[14,20,21] Thus, the cellular uptake of the RGD (−) and RGD (+) micelles into the HeLa cells was evaluated using a system loaded with ^{32}P-labeled pDNA (Figure 3C). Regardless of ligand installation, cross-linked micelles tend to be taken up more efficiently than noncrosslinked micelles. The introduction of disulfide cross-links into the micelle core appreciably contributes to an increase in the stability of micelles under physiological conditions.[9] This implies that disulfide cross-links might prevent the micelles from dissociation in the extracellular medium, and consequently facilitate their internalization into the cellular compartment. Interestingly, there is no significant increase in micelle uptake even by installing RGD ligands, suggesting that other factors, including modulation of intracellular trafficking, may be involved in the enhancement of transfection efficiency by cyclic RGD peptide ligands.

Intracellular Distribution of Polyplex Micelles. Our previous report showed that RGD (+) polyplex micelles preferentially localize in the perinuclear region, unlike RGD (−) polyplex micelles,[11] suggesting that RGD ligands likely modulate intracellular trafficking of polyplex micelles. Therefore, detailed observation of the intracellular distribution was carried out using CLSM (Figure 4). The medium was replaced with fresh medium after 1 h incubation of polyplex micelles with cultured HeLa cells. Then CLSM observation was carried out after each reincubation without polyplex micelles in the medium. The CLSM images are shown in Figure 4A. The micelles localized in the inner-cytoplasm were quantitatively evaluated using the procedure described in the Experimental Section and shown in Figure 4B; the data are summarized in Figure 4C. After the 5 h reincubation (total 6 h incubation), the spots observed in the inner region of the cytoplasm were mainly the green spots of RGD (+) micelles (Figure 4A, left). On the other hand, the RGD (−) micelles, shown in red stayed mainly near the cell membrane (Figure 4A, left), but some fraction was observed in the inner-cytoplasm as red spots (RGD (−) micelle alone) or yellow spots (colocalizing with RGD (+) micelles). In the early stages, almost half of the cell population with fluorescence had only green spots, corresponding to the internalization of RGD (+) micelles (Figure 4C); this indicated that RGD (+) micelles were internalized into the inner-cytoplasm much faster than RGD (−) micelles. However, further reincubation resulted in the decrease in the cell fraction that showed only green spots and lead to an increase in the fraction that included yellow spots, corresponding to the colocalization of RGD (−) and RGD (+) micelles, as well as to an increase in red spots, corresponding to the presence of RGD (−) micelles alone. Note that there are two possibilities for the appearance of yellow spots. The first is that RGD (−) and RGD (+) micelles adsorbing to the cell membrane were simultaneously endocytosed by the cell. The second is that RGD (−) and RGD (+) micelles that were separately internalized into the cells subsequently colocalized through the possible fusion of the compartments in the inner-cytoplasm. On the other hand, the green spots still existed in a definite fraction of cells (G + GY + GRY) even after long-term reincubation, while the fraction of the cells including red spots (R + RY + GRY) continued to increase (Figure 4C). Thus, it is reasonable to assume that there may be distinct routes of internalization for RGD (−) and RGD (+) micelles, and eventually their final destinations may be different.

To examine whether or not RGD ligand installation in the micelles alters their intracellular trafficking, organelles were selectively stained using LysoTracker for the late endosomes and the lysosomes, and CT-B for the lipid rafts and the caveosomes (Figures 5 and 6).[22,23] In this experiment, the medium was replaced 1 h after the addition of polyplex micelles, followed by 11 h of reincubation. The rate of colocalization was quantified by the formula shown in the Experimental Section. The experiment with LysoTracker revealed that 39% of RGD (−) micelles and 28% of RGD (+) micelles in the inner-cytoplasm were localized in the late endosomes and lysosomes, indicating that the colocalization ratio of RGD (−) micelles with the late endosomes and lysosomes was significantly higher than that of RGD (+) micelles ($P = 0.0052$) (Figure 5B). On the other hand, the observation with CT-B revealed that 22% of RGD (−)

(20) de Bruin, K.; Ruthardt, N.; von Gersdorff, K.; Bausinger, R.; Wagner, E.; Ogris, M.; Bräuchle, C. Cellular Dynamics of EGF Receptor-Targeted Synthetic Viruses. *Mol. Ther.* **2007**, *15*, 1297–1305.

(21) Vinogradov, S.; Batrakova, E.; Li, S.; Kabanov, A. Polyion Complex Micelles with Protein-Modified Corona for Receptor-Mediated Delivery of Oligonucleotides into Cells. *Bioconjugate Chem.* **1999**, *10*, 851–860.

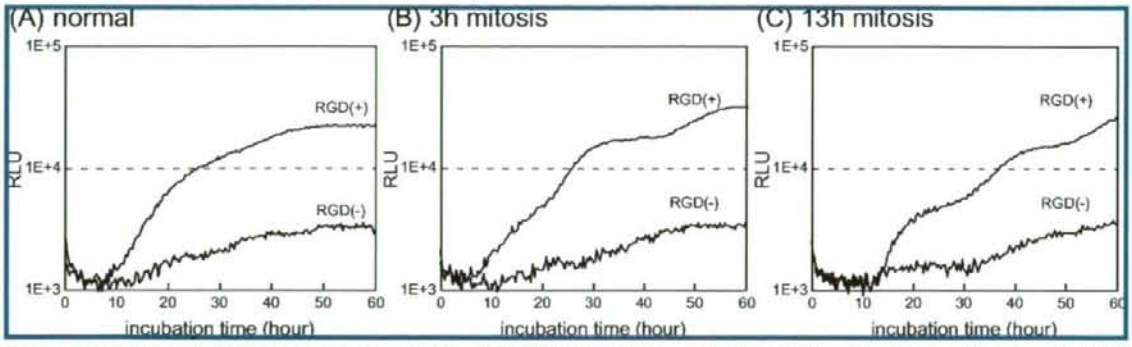

Figure 7. Real-time luciferase gene expression of B-SH11% polyplex micelles (N/P = 2) with or without cyclic RGD peptide ligands under the "normal" condition (A), the "3 h mitosis" condition (B), and the "13 h mitosis" condition (C).

micelles and 44% of RGD (+) micelles in the inner-cytoplasm were localized in the lipid rafts and caveosomes, respectively, indicating that the RGD (+) micelles had significantly higher localization ratios to the lipid rafts and caveosomes than the RGD (−) micelles ($P = 0.0004$) (Figure 6B). These results indicate that the polyplex micelles with cyclic RGD ligands were internalized preferentially through caveolae-mediated endocytosis by HeLa cells.

Real Time Luciferase Gene Expression. In the conventional luciferase assay, transfected cells need to be lysed before measurement, and this restricts the evaluation of luciferase expression in real time. Alternatively, as explained in the Experimental Section, Kronos Dio allows us to measure real-time luciferase expression while maintaining the cell culture for a prolonged period.[24] Figure 7 shows the results of time-dependent gene expression with RGD (−) and RGD (+) B-SH11% micelles. Under the "normal" condition without any control over the cell cycle (Figure 7A), the luciferase expression with RGD (−) and RGD (+) micelles started almost simultaneously around 8 h after the micelles were added. The expression of genes reached a plateau after around 50 h of incubation regardless of the presence of RGD ligands. Considering that the half-life of luciferase is about 2−3 h in living cells,[25] the rate of luciferase production is expected to be equal to that of luciferase degradation in regions over 50 h. RGD (+) micelles showed higher transfection rates than RGD (−) micelles at all time points. Real-time gene expression was assessed for cells after aphidicolin, a DNA synthesis inhibitor, was used to synchronize the cell cycle (Figures 7B and 7C). HeLa cells incubated with aphidicolin for more than 16 h are arrested between the G1 and S phases,[17] and a change to a medium that dose not contain aphidicolin allows HeLa cells to progress into the S phase to divide 13 h later. We confirmed that almost all HeLa cells were in the S phase immediately after the medium replacement and were in the G2 phase 10 h after the replacement (data not shown). Under the "3 h mitosis" condition, where cell division started 3 h after polyplex micelles were added (Figure 7B), gene expression by RGD (+) micelles was detected 5 h after incubation, while that of RGD (−) micelles was below the Kronos Dio detection limit even after about 12 h of incubation. This implies that RGD (+) micelles can migrate into the nucleus during the first mitosis due to their early accumulation in the perinuclear region, whereas this is not the case for RGD (−) micelles because of their slow accumulation in that region. Under the "13 h mitosis" condition, where cell division started 13 h after polyplex micelles were added (Figure 7C), luciferase expression with RGD (−) and RGD (+) micelles was detected simultaneously at 13 h after incubation, which corresponds to the initiation of cell division. This result suggests that RGD (+) micelles move early to the perinuclear region but may not be actively transported into the nucleus in the nonmitotic condition. As shown in Figure 4, most of the RGD (−) micelles were internalized into the cell to accumulate in the perinuclear region at a level comparable to that of RGD (+) micelles after 24 h of incubation. Nevertheless, RGD (−) micelles under the "13 h mitosis" condition exhibited remarkably lower increases in luciferase expression at more than 30 h of incubation compared to RGD (+) micelles. Apparently, this cannot be explained by the difference in the migration rate between RGD (−) and RGD (+) micelles because of their similar levels of accumulation in the perinuclear region in this time period. Presumably, this might be explained by the difference in the final destinations of the polyplex micelles with and without cyclic RGD ligands due to the modulation of intracellular trafficking as shown in Figures 5 and 6.

(22) Orlandi, P. A.; Fishman, P. H. Filipin-Dependent Inhibition of Cholera Toxin: Evidence for Toxin Internalization and Activation through Caveolae-Like Domains. *J. Cell Biol.* **1998**, *141*, 905–915.

(23) von Gersdorff, K.; Sanders, N. N.; Vandenbroucke, R.; de Smedt, S. C.; Wagner, E.; Ogris, M. The Internalization Route Resulting in Successful Gene Expression Depends on both Cell Line and Polyethylenimine Polyplex Type. *Mol. Ther.* **2006**, *14*, 745–753.

(24) Takae, S.; Miyata, K.; Oba, M.; Ishii, T.; Nishiyama, N.; Itaka, K.; Yamasaki, Y.; Koyama, H.; Kataoka, K. PEG-Detachable Polyplex Micelles Based on Disulfide-Linked Block Catiomers as Bioresponsive Nonviral Gene Vectors. *J. Am. Chem. Soc.* **2008**, *130*, 6001–6009.

(25) Ignowski, J. M.; Schaffer, D. V. Kinetic Analysis and Modeling of Firefly Luciferase as a Quantitative Reporter Gene in Live Mammalian Cells. *Biotechnol. Bioeng.* **2004**, *86*, 827–834.

Discussion

In the present study, two distinctive implementations, that of environment-sensitive cross-links in the core and that of cyclic RGD peptide ligands on the surface, were integrated into the polyplex micelles formed by PEG-PLys block copolymers and pDNA. The physicochemical characteristics of these micelles were quite similar regardless of the thiolation degree or the introduction of RGD ligands (Table 1). The PEG palisade surrounding the polyplex core shielded the charges of the micelles to maintain very small absolute values in the ζ-potentials. The cumulant diameter of polyplex micelles was around 100 nm. This indicates that all of the polyplex micelles possess favorable characteristics relevant to future *in vivo* application. In transfection experiments using cultured cells, polyplex micelles with cyclic RGD ligands achieved higher transfection efficiency than polyplex micelles without cyclic RGD ligands against HeLa cells appreciably expressing $\alpha_v\beta_3$ integrin receptors (Figure 3A). Interestingly, RGD ligands' effect on transfection was further enhanced by the introduction of disulfide cross-linking in the micelle core. Disulfide cross-links have been reported to stabilize polyplex micelles against the counter polyanion exchange reaction under nonreductive conditions.[9] Therefore, cross-linked micelles might acquire greater stability in the medium compared to noncrosslinked micelles, indicating the enhanced effect of cyclic RGD ligands. Note that RGD (+) B-SH5% micelles achieved the highest transfection efficiency among all micelles. Excessive cross-linking into the cores of polyplex micelles has been reported to overstabilize the micelles and impede the release of pDNA,[9] which is considered to be a cause of the lower transfection efficiency of B-SH11% micelles compared to that of B-SH5% micelles. The inhibitory experiment using free cyclic RGD peptides (Figure 3B) certainly confirmed that receptor-mediated uptake by RGD ligands contributed to the enhancement of gene expression. It is worth noting that the enhancement was not due to an increase in the cellular uptake of polyplex micelles (Figure 3C), suggesting that cyclic RGD peptide ligands may modulate the intracellular trafficking of the polyplex micelles, leading to increased transfection efficiency. In this regard it should be noted that, in our previous study, cyclic RGD ligands facilitated the transport of the polyplex micelles to the perinuclear region.[11] Other studies found that some ligands, such as b-FGF[26] and lactose,[27] contribute to the change in the intracellular trafficking of gene vectors. Time-dependent CLSM observation revealed that RGD (+) micelles were internalized into the cytoplasm and moved to the perinuclear region much earlier than RGD (−) micelles (Figure 4). This is consistent with the results of real-time luciferase expression under the "3 h mitosis" condition, where RGD (+) micelles exhibited earlier onset of gene expression with high efficiency (Figure 7B). The CLSM observation also clarified the variation in final localization in the cytoplasm between the two micelles (Figure 4). CLSM observation with the staining of acidic endosomes and lysosomes (Figure 5) or lipid rafts and caveosomes (Figure 6) revealed that RGD (+) micelles were distributed in the acidic organelles at lower levels than RGD (−) micelles, and were preferentially internalized via caveolae-mediated endocytosis. Considering that pDNA degradation occurs in late endosomes and lysosomes by enzymatic hydrolysis, RGD (+) micelles are more likely than RGD (−) micelles to protect entrapped pDNA from enzymatic degradation. It is known that cells uptake particles of different sizes through different routes: macropinocytosis (>200 nm), clathrin-mediated endocytosis (100−200 nm), and caveolae-mediated endocytosis (<100 nm).[28] The average particle size of RGD (−) and RGD (+) micelles was around 110 nm, with a moderate size distribution (polydispersity index = 0.14−0.18). Thus, these micelles are likely to be internalized by both clathrin- and caveolae-mediated endocytosis. Also, cyclic RGD peptides selectively recognize both $\alpha_v\beta_3$ and $\alpha_v\beta_5$ integrin receptors. $\alpha_v\beta_5$ integrins, which adenoviruses use for their internalization into target cells, are known to facilitate clathrin-mediated endocytosis,[29] while $\alpha_v\beta_3$ integrin-mediated internalization occurs via caveolae-mediated endosytosis.[30,31] Since $\alpha_v\beta_3$ integrins have 10-times higher binding affinity to cyclic RGD peptides than $\alpha_v\beta_5$ integrins,[32] it is reasonable to assume that RGD (+) micelles might preferably recognize $\alpha_v\beta_3$ integrins and thus to induce the caveolae-mediated endocytosis as the internalization route into HeLa cells. Alternatively, RGD (−) micelles, based on their size, might be primarily internalized by clathrin-mediated endocytosis and subsequently delivered to the acidic compartment of a lysosome. Caveolae-mediated endocytosis is not associated with a pH decrease, and is

(26) Fisher, K. D.; Ulbrich, K.; Subr, V.; Ward, C. M.; Mautner, V.; Blankey, D.; Seymour, L. W. A Versatile System for Receptor-Mediated Gene Delivery Permits Increased Entry of DNA into Target Cells, Enhanced Delivery to the Nucleus and Elevated Rates of Transgene Expression. *Gene Ther.* **2000**, *7*, 1337–1343.

(27) Hashimoto, M.; Morimoto, M.; Saimoto, H.; Shigemasa, Y.; Sato, T. Lactosylated Chitosan for DNA Delivery into Hepatocytes: The Effect of Lactosylation on the Physicochemical Properties and Intracellular Trafficking of pDNA/Chitosan Complexes. *Bioconjugate Chem.* **2006**, *17*, 309–316.

(28) Grosse, S.; Aron, Y.; Thevenot, G.; Francois, D.; Monsigny, M.; Fajac, I. Potocytosis and Cellular Exit of Complexes as Cellular Pathways for Gene Delivery by Polycations. *J. Gene Med.* **2005**, *7*, 1275–1286.

(29) Wickman, T. J.; Filardo, E. J.; Cheresh, D. A.; Nemerow, G. R. Integrin $\alpha_v\beta_5$ Selectively Promotes Adenovirus Mediated Cell Membrane Permeabilization. *J. Cell Biol.* **1994**, *127*, 257–264.

(30) Wary, K. K.; Mainiero, F.; Isakoff, S. J.; Marcantonio, E. E.; Giancotti, F. G. The Adaptor Protein Shc Couples a Class of Integrins to the Control of Cell Cycle Progression. *Cell* **1996**, *87*, 733–743.

(31) Wary, K. K.; Mariotti, A.; Zurzolo, C.; Giancotti, F. G. A Requirement for Caveolin-1 and Associated Kinase Fyn in Integrin Signaling and Anchorage-Dependent Cell Growth. *Cell* **1998**, *94*, 625–634.

(32) Marinelli, L.; Gottschalk, K.-E.; Meyer, A.; Novellino, E.; Kessler, H. Human Integrin $\alpha_v\beta_5$: Homology Modeling and Ligand Binding. *J. Med. Chem.* **2004**, *47*, 4166–4177.

known to be a nondigestive route of external substances into the cellular compartment.[33] Some nonenveloped viruses, such as simian virus 40, utilize this route for transfection to host cells and accumulate in a smooth endoplasmic reticulum compartment.[34,35] Thus, RGD (+) micelles internalized by caveolae-mediated endocytosis may be able to avoid pDNA degradation in acidic organelles, leading to high transfection efficiency. Moreover, as seen in the real-time luciferase assay under the "13 h mitosis" condition (Figure 7C), the luciferase expression of RGD•(+) micelles detected at 30 h was remarkably higher than that of RGD (−) micelles, despite the comparable levels of cellular uptake between the two (Figures 3C and 4). Obviously, this result cannot be explained by the difference in the migration rate, because there was sufficient time for both RGD (+) and RGD (−) micelles to accumulate in the perinuclear region before mitosis. The higher gene expression of RGD (+) micelles is consistent with their preferential localization in caveosomes due to distinctive intracellular trafficking through the nonacidic and nondegradable route of caveolae-mediated endocytosis.

It should be noted that the results in Figures 5 and 6 indicate that not all of the RGD (+) micelles were internalized by caveolae-mediated endocytosis. Clathrin-mediated endocytosis, a relatively slow uptake pathway, could also contribute to the internalization of a portion of RGD (+) micelles, possibly due to the nonspecific interaction between the micelle and the cell membrane, even though polyplex micelles are covered with PEG to minimize nonspecific interaction. Nevertheless, the ζ-potentials of the polyplex micelles still take small positive values, suggesting that PEG charge shielding is incomplete. This slight positive charge might induce the nonspecific interaction of polyplex micelles with the negatively charged cell membrane. If this is the case, an increase in the PEG density of polyplex micelles may reduce the interaction, increasing the ligand's effects on the uptake and gene expression of polyplex micelles. An alternative explanation on the nonspecific uptake of polyplex micelles is available by considering the amphiphilic character of the PEG molecule. A PEG chain under concentrated conditions, as found in the shell layer in the micelle system, might have the ability to interact with the plasma membrane components through hydrophobic interaction or indirectly through a bridge of hydrated water molecules.[36] Research to clarify the underlying mechanism is now under way in our laboratory, and the results will be reported elsewhere in the near future.

Conclusions

In conclusion, polyplex micelles with integrated implementations of cyclic RGD peptide ligands on the micelle surface and disulfide cross-linking in the core achieved remarkably enhanced transfection efficiency against HeLa cells expressing $\alpha_v\beta_3$ integrins on the surface. The RGD ligands were effective not for increasing uptake but for modulating intracellular trafficking of polyplex micelles. RGD (+) micelles were distributed in the perinuclear region at an early period and were preferentially internalized by caveolae-mediated endocytosis via nonacidic and nondegradable intracellular compartments. These results indicate that polyplex micelles with cyclic RGD ligands and disulfide cross-links are promising approaches to facilitate cell-specific transfection by controlling intracellular trafficking as well as by the environment-sensitive release of encapsulated pDNA in the target cells.

Cyclic RGD peptide is well-known to selectively recognize $\alpha_v\beta_3$ integrin receptors identified as a marker of angiogenic vascular tissue,[37] and thus is a good candidate as a ligand for gene vectors used for diseases including tumor characterized by neovascularization. Indeed, nonviral gene vectors, in which cyclic RGD peptide ligands are installed have been applied to delivery pDNA and siRNA to tumor vasculature, effectively suppressing tumor growth.[13,14] Thus, polyplex micelle with cyclic RGD ligands and disulfide cross-links may be a useful system for cancer gene therapy through a systemic administration.

Acknowledgment. This work was financially supported in part by the Core Research Program for Evolutional Science and Technology (CREST) from Japan Science and Technology Corporation (JST), by Special Coordination Funds for Promoting Science and Technology (SCF) commissioned by the Ministry of Education, Culture, Sports, Science, and Technology (MEXT) of Japan, and by Grant-in-Aid for Nanomedicine Research from the Ministry of Health, Labour and Welfare (MHLW), Japan.

MP800070S

(33) Pelkmans, L.; Kartenbeck, J.; Helenius, A. Caveolar Endocytosis of Simian Virus 40 Reveals a New Two-Step Vesicular-Transport Pathway to the ER. *Nat. Cell Biol.* **2001**, *3*, 473–483.

(34) Norkin, L. C.; erson, H. A.; Wolfrom, S. A.; Oppenheim, A. Caveolar Endocytosis of Simian Virus 40 Is Followed by Brefeldin A-Sensitive Transport to the Endoplasmic Reticulum, Where the Virus Disassembles. *J. Virol.* **2002**, *76*, 5156–5166.

(35) Conner, S. D.; Schmid, S. L. Regulated Portals of Entry into the Cell. *Nature* **2003**, *422*, 37–44.

(36) Kataoka, K.; Kwon, G. S.; Yokoyama, M.; Okano, T.; Sakurai, Y. Block Copolymer Micelles as Vehicles for Drug Delivery. *J. Controlled Release* **1993**, *24*, 119–132.

(37) Brooks, P. C.; Clark, R. A.; Cherish, D. A. Requirement of Vascular Integrin $\alpha_v\beta_3$ for Angiogenesis. *Science* **1994**, *264*, 569–571.

Enhancement of Angiogenesis Through Stabilization of Hypoxia-inducible Factor-1 by Silencing Prolyl Hydroxylase Domain-2 Gene

Shourong Wu[1,2], Nobuhiro Nishiyama[1,3], Mitsunobu R Kano[3,4], Yasuyuki Morishita[4], Kohei Miyazono[4], Keiji Itaka[1], Ung-il Chung[1,3,5] and Kazunori Kataoka[1,3,6]

[1]Division of Clinical Biotechnology, Center for Disease Biology and Integrative Medicine, Graduate School of Medicine, The University of Tokyo, Tokyo, Japan; [2]Department of Chemistry and Biotechnology, Graduate School of Engineering, The University of Tokyo, Tokyo, Japan; [3]Center for NanoBio Integration, The University of Tokyo, Tokyo, Japan; [4]Department of Molecular Pathology, Graduate School of Medicine, The University of Tokyo, Tokyo, Japan; [5]Department of Bioengineering, Graduate School of Engineering, The University of Tokyo, Tokyo, Japan; [6]Department of Materials Engineering, Graduate School of Engineering, The University of Tokyo, Tokyo, Japan

Hypoxia-inducible factor-1 (HIF-1) plays a central role in cellular response to hypoxia by activating vascular endothelial growth factor (VEGF) and other angiogenic factors. Prolyl hydroxylase domain-2 (PHD2) protein induces the degradation of HIF-1 by hydroxylating specific prolyl residues. Therefore gene silencing of PHD2 by RNA interference (RNAi) might increase the expression of angiogenic growth factors and, consequently, neoangiogenesis through the stabilization of HIF-1α. In this study we have shown that the specific silencing of PHD2 is sufficient for stabilizing HIF-1α and increasing its transcriptional activity, resulting in the increased expression of angiogenic factors including VEGF and fibroblast growth factor-2 (FGF2). Moreover, when PHD2-siRNA vector was used, the increase in VEGF secretion was observed for as long as 18 days after transfection. *In vitro* treatment of human umbilical vein endothelical cells with conditioned medium from PHD2-siRNA vector-transfected NIH3T3 cells was shown to increase cell proliferation. Also, *in vivo* angiogenesis was observed in mice implanted with Matrigel plugs mixed with NIH3T3 cells transfected with PHD2-siRNA vector. These results indicate that PHD2 silencing induces expressions of multiple angiogenic growth factors by stabilizing HIF-1α, and that the implantation of cells transfected with PHD2-siRNA vector is sufficient to enhance angiogenesis *in vivo*. In the light of these findings, PHD2 silencing by RNAi might offer a potential tool for angiogenic therapy.

Received 9 October 2007; accepted 7 April 2008; published online 20 May 2008. doi:10.1038/mt.2008.90

INTRODUCTION

Therapeutic angiogenesis aims to improve neovascularization in ischemic tissues by delivery of angiogenic factors or DNA vectors encoding those proteins, such as vascular endothelial growth factor (VEGF) and fibroblast growth factor-2 (FGF2).[1–3] VEGF is produced in the early stage of the angiogenic cascade and is responsible for the initial activation of endothelial cells; this makes it an important factor in vascular development.[4] Its transgenic expression in mouse skin results in increased numbers of blood vessels that manifest excessive permeability.[5] FGF2 has been reported to act as a mitogen for both endothelial and mural cells,[6] and its role in vascular formation has also been identified.[3,7] Therapeutic angiogenesis using either VEGF or FGF2 alone has been extensively investigated. However, although phase I clinical trials had shown that their delivery was safe, phase II trials have not demonstrated efficacy as expected,[8–10] thereby suggesting that the administration of a single angiogenic growth factor might be insufficient to induce functional vessels. Therapeutic angiogenesis studies were then altered to focus on the combined application of angiogenic growth factors. The combination of VEGF and FGF2, and the combinations of each of these with other angiogenic factors such as angiopoietin-1 and platelet-derived growth factor-BB (PDGF-BB), have been reported to have potent synergistic effects on neovascularization, in both *in vitro* and *in vivo* experiments.[11–15] Collectively, these results demonstrate the complexity of the mechanism of angiogenesis, which includes the temporally and spatially orchestrated expression of multiple angiogenic factors.

Hypoxia-inducible factor-1 (HIF-1), a heterodimeric α, β transcription factor, functions as a central regulator of oxygen homeostasis, and is known to be hydroxylated on two proline residues by prolyl hydroxylase domain (PHD) prolyl hydroxylase family and degraded by E3 ubiquitin ligase complex under normoxia conditions. The inactivation of PHD2, a member of the PHD family, contributes to HIF stabilization, thereby suggesting that PHD2 is the key HIF prolyl hydroxylase.[16] More than 60 HIF-1 target genes, including VEGF and other angiogenic factors, have been identified.[17] In this context, transgenic expression of HIF-1α in mouse skin was shown to increase vascularization without excessive permeability,[18] and the expression of its constitutively active form is sufficient to induce angiogenesis in nonischemic tissue.[19]

Correspondence: Kazunori Kataoka, Department of Materials Engineering, Graduate School of Engineering, The University of Tokyo, 7-3-1 Hongo, Bunkyo-ku, Tokyo 113-8656, Japan. E-mail: kataoka@bmw.t.u-tokyo.ac.jp

RNA interference (RNAi) is a post-transcriptional gene-silencing phenomenon triggered by double-stranded RNA discovered in 1998 (ref. 20). Owing to its great specificity and efficiency, RNAi has become a powerful tool in studying gene functions, and has been extensively investigated as a therapeutic tool.[21,22] Several therapy applications are currently under clinical development.[23,24]

In this study we explored the potential for therapeutic angiogenesis using PHD2-suppressing RNAi. We demonstrated *in vitro* that PHD2 silencing upregulates the expression of multiple angiogenic growth factors. We also showed that *in vivo* implantation of PHD2-silenced cells is sufficient to enhance angiogenesis in an experimental animal model. These results have implications for the application of PHD2-suppressing RNAi in therapeutic angiogenesis.

RESULTS

Construction of pshRNAs against murine PHD2, and PHD2 gene silencing

The RNAi effect of small-interfering RNA (siRNA) is highly dependent on the sequence of the target gene. Therefore we selected two siRNAs with different sequences[25,26] and a siPHD2-pool containing four kinds of PHD2-suppressing siRNAs. All the PHD2-suppressing siRNAs clearly showed suppressive effects, with siPHD2-A showing the strongest such effect (**Figure 1a**). In order to further determine their functional effect, we investigated the efficacy of siPHD2s on HIF-1 transcriptional activity. Under normoxia conditions, both siPHD2-A-transfected NIH3T3 and C2C12 cells exhibited a significant increase in HIF-1 transcriptional activity (**Supplementary Figure S1a and b**). Consistently, in term of increasing VEGF mRNA level and protein secretion, siPHD2-A was more potent than the others (**Supplementary Figures S2 and S3**). Consistent with the decrease of its suppressive effect at 72 hours after transfection (**Figure 1a**), the effect of siPHD2 on the increase of VEGF secretion also decreased at 96 hours after transfection (**Supplementary Figure S3**). In order to obtain a long-term silencing effect, we constructed the siPHD2 expression vectors U6-pshPHD2-A, U6-pshPHD2-B, CMV-pshPHD2-A, and CMV-pshPHD2-B. U6-pshPHD2-A and CMV-psh-PHD2-A suppressed the expression of PHD2 mRNA more potently (**Figure 1b** and **c**, 90 and >60%, respectively) than the U6-shPHD2-B and CMV-psh-PHD2-B did (60 and >40%, respectively). Next, using a 5× hypoxia-responsive element promoter-driven firefly luciferase reporter (5×HRE reporter), we investigated the effect of PHD2- and PHD3 silencing on HIF-1 transcriptional activity. Under normoxia conditions, the transcriptional activity of HIF-1 was induced by pshPHD2-A vectors but not by pshPHD3 vectors (**Figure 1d** and **e**). Moreover, because U6 promoter-driven siPHD2 expression vectors showed more potent suppressive effects and induction of HIF-1 transcriptional activity than those using a cytomegalovirus (CMV) promoter, we used U6-pshPHD2-A for performing further *in vitro* and *in vivo* experiments. In addition, the suppressive effect on PHD2 by U6-pshPHD2-A persisted at>90% at 72 hours after transfection (**Figure 1f**), thereby indicating that, for achieving long-term effects, pshRNA expression vector was more potent than siRNA.

Effects of PHD2 silencing on HIF-1α protein level and HIF-1 transcriptional activity

In a normoxia environment, hydroxylation of HIF-1α protein by PHD2 resulted in the proteasomal degradation of HIF-1α.[27] This finding confirmed the effect of PHD2 silencing on HIF-1α protein. HIF-1α protein increased significantly in PHD2-silenced cells as compared to control cells (**Figure 2a**). Consistent with the earlier report, the results also showed that PHD2 silencing did not affect HIF-2α protein levels (**Figure 2a**).[16] Moreover, PHD2 silencing did not alter HIF-1α distribution in nuclei and cytoplasm (**Figure 2a** and **b**, respectively); rather, it increased the amount of HIF-1α protein in the nuclei predominantly, and an even greater increase was observed in PHD2-silenced cells exposed to conditions of hypoxia (**Figure 2c**). That is, the transcriptional activity of HIF-1 was higher when PHD2 was silenced, under both normoxia and hypoxia conditions (**Figure 2d**).

Regulation of expression of various angiogenic growth factors by silencing of PHD2

Next we analyzed whether PHD2 silencing could regulate the expression of multiple genes encoding angiogenic growth factors. The endogenous HIF-1α mRNA level in PHD2-silenced cells